AD NUMBER

AD893254

NEW LIMITATION CHANGE

TO

Approved for public release, distribution unlimited

FROM

Distribution authorized to U.S. Gov't. agencies only; Test and Evaluation; 10 SEP 1971. Other requests shall be referred to Air Force Flight Dynamics Laboratory, Attn: FER, Wright-Patterson AFB, OH 45433.

AUTHORITY

AFFDL ltr, 11 Jan 1974

AFFDL-TR-71-35, VOL. I

ANALYSIS OF THE SUPERSONIC FLOW FIELD ABOUT A FOREBODY-DECELERATOR COMBINATION

Theoretical Methods and Result Comparisons

R. A. NOREEN
L. W. RUST, JR.
P. P. RAO

UNIVERSITY OF MINNESOTA

TECHNICAL REPORT AFFDL-TR-71-35, VOL. I

MARCH 1972

AIR FORCE FLIGHT DYNAMICS LABORATORY
AIR FORCE SYSTEMS COMMAND
WRIGHT-PATTERSON AIR FORCE BASE, OHIO

NOTICES

When Government drawings, specifications, or other data are used for any purpose other than in connection with a definitely related Government procurement operation, the United States Government thereby incurs no responsibility nor any obligation whatsoever; and the fact that the Government may have formulated, furnished, or in any way supplied the said drawings, specifications, or other data, is not to be regarded by implication or otherwise as in any manner licensing the holder or any other person or corporation, or conveying any rights or permission to manufacture, use, or sell any patented invention that may in any way be related thereto.

Copies of this report should not be returned unless return is required by security considerations, contractual obligations, or notice on a specific document.

ANALYSIS OF THE SUPERSONIC FLOW FIELD ABOUT A FOREBODY-DECELERATOR COMBINATION

Theoretical Methods and Result Comparisons

R. A. NOREEN
L. W. RUST, JR.
P. P. RAO

UNIVERSITY OF MINNESOTA

FOREWORD

This report was prepared by the Department of Aerospace Engineering and Mechanics of the University of Minnesota in compliance with U. S. Air Force Contract No. F33615-68-C-1227, "Theoretical Deployable Aerodynamic Decelerator Investigations," Task 606503, "Parachute Aerodynamics and Structures," Project 6065, "Performance and Design of Deployable Aerodynamic Decelerators," Prof. H. G. Heinrich, Principal Investigator. The work on this report was performed between December 16, 1967, and October 15, 1969.

The work accomplished under this contract was sponsored jointly by U. S. Army Natick Laboratories, Department of the Army; Bureau of Aeronautics and Bureau of Ordnance, Department of the Navy; and Air Force Systems Command, Department of the Air Force, and was directed by a Tri-Service Steering Committee concerned with Aerodynamic Retardation. The work was administered under the direction of the Recovery and Crew Station Branch, Air Force Flight Dynamics Laboratory, Air Force Systems Command. Mr. James H. DeWeese was the project engineer.

Volume I of this report contains discussion of the analytical methods and comparison of the calculations with experimental measurements.

Volume II of this report contains details of the calculation procedures and computer program.

The authors wish to express their gratitude to Mr. Charles Babish of the Air Force Flight Dynamics Laboratory for his many constructive suggestions, and to the staff and students of the Department of Aerospace Engineering and Mechanics who helped in the accomplishment of this study and to the North Star Research and Development Center for their cooperation in permitting Dr. L. W. Rust, Jr., to participate in various objectives of this project.

This report was submitted by the authors in January, 1971.

This technical report has been reviewed and is approved.

GEORGE A. SOLT, JR.
Chief, Recovery and Crew Station Branch
Air Force Flight Dynamics Laboratory

ABSTRACT

The supersonic flow field about a forebody-decelerator combination is analyzed. Tangent-cone and Newtonian methods are used to predict forebody surface pressures. Empirical correlations based on local similarity solutions predict the boundary layer characteristics, and boundary layer similarity techniques are used to predict the forebody wake parameters. The flow about a conical secondary body in the forebody wake is calculated using the method of characteristics. In Volume I the methods are presented and explained, and the results of the calculations are compared with experimental measurements; in Volume II the details of the calculation procedure and computer program are presented.

TABLE OF CONTENTS

TABLE OF CONTENTS (CONT.)

ILLUSTRATIONS

ILLUSTRATIONS (CONT.)

SYMBOLS

A	$A = 1 - \frac{u^2}{a^2}$, in Eqns 89 and 90
a	speed of sound
a_o, a_1, a_2, a_3, a_4	coefficients in velocity profile, Eqn 26
a_o	stagnation condition speed of sound
B	exponent in Eqn 17, defined in Eqn 18
B	$B = -\frac{uv}{a^2}$, in Eqns 89 and 90
C	$C = 1 - \frac{v^2}{a^2}$, in Eqns 89 and 90
C_p	pressure coefficient
c_p	specific heat at constant pressure
D	forebody diameter
D	$D = \frac{\gamma_r}{r} + \frac{r}{V}\left[2h_o - V^2\right]^{\frac{1}{\gamma-1}} \frac{dh_o}{dn} - \frac{\gamma-1}{2\gamma}\frac{r}{V}\left[2h_o - V^2\right]^{\frac{\gamma}{\gamma-1}} \cdot \left[1 - \frac{V^2}{a^2}\right] \frac{d\left(\frac{S}{R}\right)}{dn}$, in Eqns 89 and 90
D_B	forebody base diameter
f	function defined in Eqn 79
h	enthalpy
$\hat{i}$	unit vector in x direction
$\hat{j}$	unit vector in y direction
K	exponent in Eqn 12
k	turbulence constant in Eqn 44
$\hat{k}$	unit vector normal to x-y plane
L	body length

ℓ	axial distance measured from forebody base
ℓ/D_B	dimensionless distance from forebody base
M	Mach number
$\bar{M}_1$	effective Mach number, Eqn 48
m*	momentum defect
n	transformed coordinate, Eqn 52
$\hat{n}$	unit vector normal to a streamline
p	pressure
Pr	Prandtl number
R	gas constant
Re	Reynold's number
r	radial coordinate
r_B	base radius of forebody
r_s	radius of shock at any value of x
S	entropy
s	distance from front stagnation point measured along surface
T	temperature in degrees Rankine
t	thickness of towline
U_∞	freestream velocity
u	velocity component in x direction
V	total velocity, $V = \sqrt{u^2 + v^2}$
v	velocity component in r direction
X	axial distance downstream measured from forebody wake stagnation point
x	axial distance downstream measured from forebody nose; also used for axial length measurement for either body

x_o	axial location of forebody wake stagnation point
β	shock angle
β	pressure gradient parameter, Eqn 13
γ	ratio of specific heats
Δ	transformed wake thickness
δ	wake radius or thickness, boundary layer thickness (Fig 7)
δ^*	wake displacement thickness
η	transformed non-dimensional coordinate, Eqn 24
θ	boundary layer momentum thickness, also flow angle
θ_{tr}	transformed momentum thickness
λ	slope of characteristic line
μ	dynamic viscosity coefficient
μ	Mach angle
ν	kinematic viscosity coefficient
ξ	wake form parameter
ξ^*	effective surface distance, Eqn 14
ξ^*_T	turbulent effective surface distance, Eqn 17
ρ	density
σ	local inclination angle of forebody surface
σ_c	critical cone half-angle of forebody surface
$\bar{\sigma}$	effective cone half-angle
τ	body thickness ratio
ψ	stream function
ω	vorticity

Subscripts:

a	adiabatic
B	condition at base of forebody
char	condition on a characteristic line
cl	condition at wake centerline
cr	condition at $Re = Re_{critical}$
e	condition at boundary layer edge
i	condition at i^{th} station
i + 1	condition at $(i + 1)^{th}$ station
o	stagnation or total value of parameters
r	partial derivative of function with respect to r
ref	reference value of parameter
s	condition at forebody nose stagnation point
TR	condition at transition point
w	wake condition
x	partial derivative of function with respect to x
δ_{DTR}	diameter of wake at transition point
θ_{cr}	momentum thickness at which boundary layer becomes unstable
θ_{TR}	momentum thickness at transition
1	viscous wake edge condition
1	condition on characteristic curve 1 or at point 1
2	condition on characteristic curve 2 or at point 2
12	condition along line connecting points 1 and 2
∞	freestream condition

Superscripts:

—	indicates average value of function
→	indicates a vector function

I. INTRODUCTION

This report presents the results of an effort to calculate the flow field characteristics of a two-body trailing decelerator system in supersonic flow (Fig 1). The report is divided into two volumes, the first dealing with theoretical methods and a comparison of the results of a sample calculation with measurements, the second presents and explains the computer program used for the calculations.

This volume, Volume I, presents an explanation of the methods used to analyze the forebody (the object to be decelerated or payload), the trailing secondary body (the decelerator) (Fig 1), and the comparison of results with experimentally measured values. Naturally, the ideal objective would be to have a theory and methods that provide a complete closed solution to the entire flow field about the two bodies. Within the current state of the art, however, this goal cannot be achieved. These efforts have been directed at utilizing tractable methods with limited assumptions and required inputs that provide very useful results. Wherever assumptions are necessary, they are discussed in detail and their effects evaluated where possible.

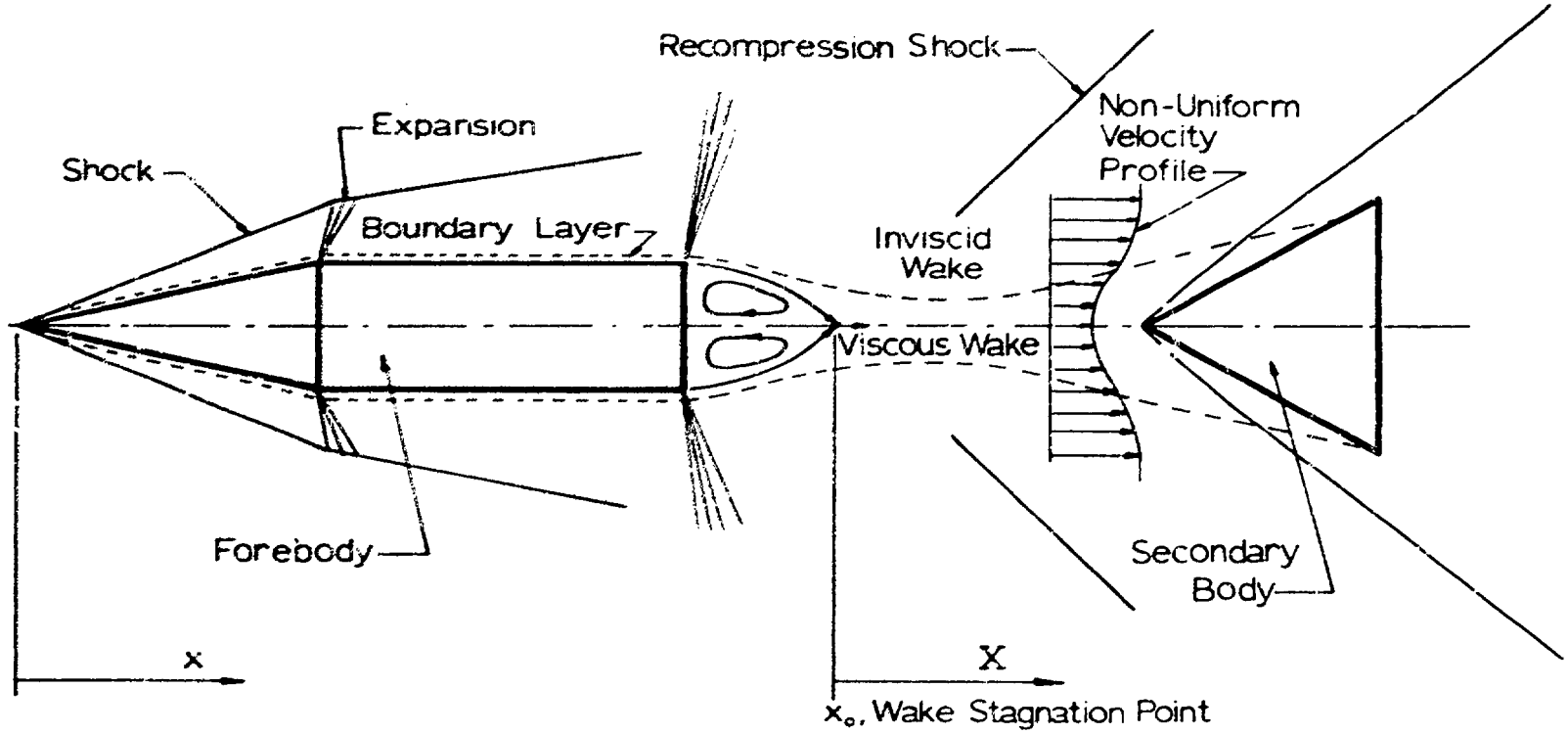

Fig 1 Schematic of Flow Field of the Two Body Deceleration System

II. FOREBODY AND WAKE ANALYSIS

This division describes the analysis used to predict the flow characteristics about the forebody and its wake, and draws heavily on the work presented in Ref 1, in particular Section B, the explanation of the analysis. In view of this, the matter presented in this section is not, nor is it intended to be, rigorously complete; rather it should provide a basic understanding of the analysis. For further details or information Ref 1 must be consulted.

A. Extent of Analysis, Required Inputs, and Results

1. Extent of Analysis

The forebody and wake analysis examines the flow about the forebody extending axially from the bow shock downstream to the secondary body bow shock, and normally from the surface of the forebody outward to its bow shock. The analysis assumes that flow conditions upstream of the forebody are uniform.

2. Required Inputs

The forebody and wake analysis requires the following:

a. freestream conditions

b. forebody geometry

c. bow shock shape and standoff distance.

3. Results

In addition to body geometry and freestream conditions, the forebody subroutine produces the calculated local static pressure, total pressure and Mach number on the body surface at various axial locations and on various planes containing, and rotated about, the axis. Since the flow characteristics at the base of the forebody are likely to be affected by a possible transition into turbulence on the body surface, the transition point location on the body surface and on various ϕ planes is also printed out. Reynold's number, based on momentum thickness, inviscid density, local inviscid velocity, local momentum defect, and momentum thickness at the base for different ϕ planes, is provided. Integration of the local momentum defect around the surface at the forebody base provides the total momentum defect, which will be used in wake computations.

Wake computations begin with forebody boundary layer and base condition inputs. The program selects either laminar or turbulent wake conditions, based on the transition Reynold's number, and prints out the input values of the viscosity model. At every ℓ/D location behind the base of the forebody and at every iteration of wake computation, values of θ/Δ, Δ/L, δ/D, δ^*, and the local inviscid velocity at the wake edge are provided. The viscous wake is specified by the values of R/D, M, M/M_∞, V/V_∞, u, p_o/p_∞, h_o/h_{oe}, and h/h_i at each axial location, ℓ/D, and radial distance η, the non-dimensional transformed radial coordinate. The inviscid wake is determined by the values of R/D, M, M/M_∞, V/V_∞, u, p_o/p_∞, p_o/p_{oe}, and T at various values of the transformed coordinate n.

B. Method and Explanation of the Forebody-Wake Analysis (from Ref 1)

1. Body to Bow Shock Region

The variations of flow properties in this region are primarily due to the changes caused by the forebody bow shock and secondary shocks such as recompression shocks and forebody flare shocks. Assuming negligible changes in entropy across the secondary shocks, total flow properties are invariant following a streamline starting from any point behind the forebody bow shock. In Ref 1, the shock shape, determined from experiments or from analytical methods for simple bodies, is represented in multiple regression curve fit form

$$\frac{r}{D_\theta} = \frac{a + b\left(\frac{x}{D_\theta}\right) + c\left(\frac{x}{D_\theta}\right)^2}{1 - d\left(\frac{x}{D_\theta}\right)} \qquad (1)$$

where a, b, c, and d are polynomial coefficients. Since the shock is completely specified, the flow properties immediately behind the shock are determined from shock jump conditions.

2. Forebody Surface Pressure Distribution

The total and static pressures on the forebody surface are estimated using Newtonian or tangent-cone methods. The forebody surface is represented by a number of x and r coordinates of points on the surface. The nose half-angle of the forebody is determined using coordinates at 0th and 1st stations where

$$\sigma_i = \tan^{-1}\left(\frac{r_{i+1} - r_i}{x_{i+1} - x_i}\right) \qquad \text{at } i = 0 \qquad (2)$$

For a given freestream Mach number an attached shock exists if the nose half-angle is less than the critical cone half-angle. The relation between critical cone half-angle and freestream Mach number (Ref 2) can be represented, after curve fitting, by

$$\sigma_c = \frac{-11.6388 + 64.3555M - 65.7643M^2 + 14.0014M^3 - 1.07148M^4}{(1 - 1.13017M)} \quad (3)$$

If the nose half-angle σ_0 from Eqn 2 is greater than or equal to the critical cone angle from Eqn 3, a detached shock exists at the apex. The apex total pressure p_s is given by normal shock relation (Ref 2)

$$p_s = p_\infty \left\{ \left[\frac{(\gamma+1) M_\infty^2}{2} \right]^\gamma \left[\frac{\gamma+1}{2\gamma M_\infty^2 - (\gamma-1)} \right] \right\}^{\frac{1}{\gamma-1}} \quad (4)$$

Static pressure can be estimated from the Newtonian method,

$$p_e = p_s \sin^2 \sigma_0 \quad (5)$$

If the nose half-angle σ_0 is less than critical cone half-angle σ_c, an attached shock exists at the apex. The flow region behind the shock is considered a conical flow region. The nose half-angle σ_0 and the freestream Mach number approximately determine the shock angle β. The velocity components along and perpendicular to any ray from the apex of the body can be determined by expanding the velocities in Taylor series and using the approximate shock angle β. The procedure is continued until the normal velocity on the body surface is evaluated. Since the boundary condition at the surface requires the normal component of velocity to be zero, the shock angle β is altered until the deviation of normal velocity from zero is within allowable limits. The surface Mach number, static pressure, and total pressure are evaluated from the above conical flow analysis.

A Newtonian or conical flow solution is used to determine the static pressure at each point on the body profile. As long as the local inclination angle σ_{i+1} of the body surface at the $(i + 1)^{th}$ station is less than or equal to the local inclination angle σ_i at the i^{th} station, no surface shock exists and total pressure remains unaltered. If the bow shock wave is detached, static pressure is obtained from the Newtonian method, until the local inclination angle σ_i is less than the critical cone half-angle σ_c beyond which the conical flow solution is used.

On the other hand, if the local inclination angle σ_{i+1} at the $(i + 1)^{th}$ station is greater than the value σ_i at the i^{th} station, a corner shock appears at the surface, and the total pressure is altered. The effective conical half-angle, $\bar{\sigma}$, is given by

$$\bar{\sigma} = \sigma_{i+1} - \sigma_i \tag{6}$$

Here again, if $\bar{\sigma}$ is greater than or equal to the critical cone half-angle σ_c corresponding to Mach number M_{ei} at the i^{th} station, the shock is detached, and the total pressure $P_{o(i+1)}$ at $(i + 1)^{th}$ station will be

$$P_{o_{(i+1)}} = P_{o_i}\left\{\left[\frac{(\gamma+1)M_{ei}^2}{(\gamma-1)M_{ei}^2+2}\right]^{\gamma}\left[\frac{\gamma+1}{2\gamma M_{ei}^2-(\gamma-1)}\right]\right\}^{\frac{1}{\gamma-1}} \tag{7}$$

The static pressure is determined from the Newtonian method,

$$P_{e_{(i+1)}} = P_{o_{(i+1)}} \sin^2\bar{\sigma} \tag{8}$$

However, if $\bar{\sigma}$ is less than critical cone half-angle σ_c corresponding to M_{ei}, the conical flow solution will be used to determine total pressure, static pressure, and surface Mach number.

3. Boundary Layer Analysis

Because of the nature of the wake analysis, IIB4, the primary aim of the boundary layer analysis is to obtain the momentum defect at the base of the forebody, which is also the only output from the computer program. Thus this boundary layer analysis is restricted to determining that quantity, and assumes that the flow properties at the edge of the boundary layer are those derived in IIB2 for forebody surface conditions.

The boundary layer momentum defect can be expressed as

$$m^* = \rho_e u_e^2 \int_0^{\infty}\int_0^{\pi} \frac{\rho u}{\rho_e u_e}\left(1 - \frac{u}{u_e}\right) r\,dr\,d\phi \tag{9}$$

Equation 9 can be recast into the form

$$m^* = \int_{circumference} \rho_e u_e^2 \theta \, ds \tag{10}$$

where ds is the circumferential increment of length. The boundary layer momentum thickness θ is defined as

$$\theta = \int_0^\infty \frac{\rho u}{\rho_e u_e} \left(1 - \frac{u}{u_e}\right) dr \tag{11}$$

Since boundary layer characteristics primarily depend on the laminar or turbulent nature of the flow on the forebody surface, the momentum thickness, θ, for these two cases is developed in the following paragraphs, a and b, and the laminar-turbulent transition is discussed in paragraph c.

a. Laminar Boundary Layer Analysis

The momentum thickness of a laminar forebody boundary layer is determined from an empirical equation which depends on edge conditions and local pressure gradient.

This effect of pressure gradient on a laminar boundary layer is usually taken in the form of the pressure gradient parameter β, which varies from one, at a two-dimensional stagnation point, to zero for a zero pressure gradient region. Although β varies from point to point on the body surface, the boundary layer characteristics largely depend on the local value of the pressure gradient parameter β. This concept of "local similarity" has been used in Ref 1 to obtain the following expression for θ:

$$\frac{\theta}{r_B} = \frac{\sqrt{2}(0.491)(1 - 0.09\beta^{.44})\,\xi^{*1/2}}{\left(\frac{\rho_e u_e r_B}{\mu}\right)^{1/2}\left(\frac{u_e}{V_\infty}\right)^{1/2}\left(\frac{p_e}{p_s}\right)^{1/2}\left(\frac{r}{r_B}\right)^{K}\left(\frac{\rho_e \mu_e}{\rho_w \mu_w}\right)^{0.114}} \tag{12}$$

where K = 0 for two-dimensional flow, and K = 1 for axisymmetric flow.

The pressure gradient parameter β is given by

$$\beta = 2\,\frac{\xi^*}{u_e}\left(\frac{\partial u_e}{\partial \xi^*}\right) \tag{13}$$

where ξ^* represents an effective surface distance considering boundary layer history up to that point,

$$\xi^* = \int_0^{S/r_B} \frac{\rho_e}{\rho_s} \frac{u_e}{V_\infty} \left(\frac{r}{r_B}\right)^{2K} d\left(S/r_B\right) \qquad (14)$$

Knowing the inviscid flow properties at the edge of the boundary layer and evaluating ξ^*, ρ and θ/r_B from Eqns 14, 13, and 12, the momentum defect at the base of the circular body can be written as

$$m^* = \pi D_B (\rho_e u_e \theta)_B \qquad (15)$$

b. Turbulent Boundary Layer Analysis

The turbulent boundary layer analysis used in Ref 1 to determine the momentum defect at the base of the forebody is mainly based on the results of Reshotko and Tucker (Ref 3). If the flow on the forebody surface is completely turbulent, the turbulent boundary layer analysis is applied from the nose stagnation point. However if the boundary layer is initially laminar, turbulent flow analysis starts from the transition point where θ turbulent = θ laminar. The transition point is located on the basis of transition Reynold's number, $Re_{\theta TR}$, discussed in Section c. In Ref 3 the presence of eddy viscosity in the turbulent boundary layer necessitates the use of an approximate equation to represent the shear stress distribution, and the effect of pressure gradient on boundary layer velocity profile is taken into account through the use of moment of momentum equation. After considerable simplification, the results of Reshotko and Tucker (Ref 3) are represented by a transformed momentum thickness θ_{tr} in the mathematical form (Ref 1)

$$\frac{\theta_{tr}}{r_B} = \left(\frac{(\theta_{tr})_{TR}}{r_B}\right)\left(\frac{\gamma_{TR}}{\gamma}\right)^K \left(\frac{(p_0)_{TR}}{p_0}\right)^{0.1775} \left(\frac{(M_e)_{TR}}{M_e}\right)^{0.8227\,B + 0.1775} + \qquad (16)$$

$$+ \left[\frac{0.01173\,\xi_T^*}{\left(\frac{M_e r_B a_0}{\nu_0}\right)^{0.2155}}\right]^{0.8227}$$

The subscript TR indicates the values at the transition point; a_o and ν_o are the velocity of sound and the kinematic viscosity at stagnation conditions of the local external stream. The turbulent distance parameter ξ_T^* is given by

$$\xi_T^* = \frac{1}{M_e^B \left(\frac{r}{r_B}\right)^{1.2155\,K}} \int_{s_1/r_B}^{S/r_B} \frac{M_e^B \left(\frac{r}{r_B}\right)^{1.2155\,K}}{\left(\frac{T_{ref}}{T_e}\right)^{0.732} \left(\frac{T_o}{T_e}\right)^{3.268}} \qquad (17)$$

The distance s_1 is the location of the transition point measured along the body surface from the front stagnation point. If the flow is completely turbulent $s_1 = 0$. The exponent B in Eqns 16 and 17 is approximated by the function:

$$B = 4.2 + 1.58\left[\frac{T_w}{T_o} - 1\right] \qquad (18)$$

where T_o is the inviscid stagnation temperature. The term $\left(\frac{T_{ref}}{T}\right)$ in Eqn 17 is given as

$$\left(\frac{T_{ref}}{T}\right) = \frac{1}{2}\left(1 + \frac{T_w}{T_e}\right) + 0.22\left(\frac{\gamma-1}{2} M_e^2 P_r^{1/3}\right) \qquad (19)$$

The actual momentum thickness θ is then evaluated from the relation

$$\theta = \theta_{tr}\left(1 + \frac{\gamma-1}{2} M_e^2\right)^3 \qquad (20)$$

The local momentum thickness θ for a turbulent boundary layer beyond the transition point can then be determined using the above equations. The momentum defect at the base of the forebody is then determined from Eqn 15.

c. Boundary Layer Transition

If the flow on body surface is initially laminar, the transition point must be located to change the calculation method from the laminar to the turbulent boundary layer analysis. The Reynold's number based on momentum thickness at the transition point can be approximated by (Ref 1)

$$Re_{\theta_{TR}} \simeq 1000(1 - 0.12M^2 + 0.023M^3)^{1/2}\left[-2.29 + 17.38\left(\frac{h_w}{h_{aw}}\right) - 18\left(\frac{h_w}{h_{aw}}\right)^2 + 3.91\left(\frac{h_w}{h_{aw}}\right)^3\right]^{1/2} \quad (21)$$

where h_w = enthalpy based on wall temperature and h_{aw} = enthalpy based on adiabatic wall temperature.

In an adverse pressure gradient region, $Re_{\theta_{TR}}$ is replaced by the critical Reynold's number, $Re_{\theta_{cr}}$, given in Ref 1

$$Re_\theta \simeq 0.163\ Re_{\theta_{TR}} \quad (22)$$

Equations 21 and 22 have been developed and discussed in greater detail in Appendix III of Ref 1. The transition point is located where the laminar θ satisfies Eqns 21 or 22.

4. Wake Analysis

a. Viscous Wake

The viscous wake can be divided into three major regions 1) the near wake, 2) the neck region and rear stagnation point, and 3) the far wake. The near wake is characterized by 1) outer rotational inviscid flow, 2) a free shear layer above the dividing stream line and 3) a recirculation region. In the near wake and wake neck region, because of the presence of a pressure gradient, the existence of a rear shock and the nonsimilar nature of the governing equations, not much success could be achieved in representing the velocity and enthalpy profiles in a mathematical form. In the far wake region assumptions such as constant momentum defect, negligible pressure gradient, and boundary layer assumptions could be used to determine the flow variables. Neglecting nonisentropic processes in the near wake region and assuming that no external work is done on the fluid, and a constant wake momentum defect, the wake momentum defect may be equated to the boundary layer momentum defect at the base of the forebody. Thus, momentum thickness, θ_1 , of the wake is given by

$$\theta_1^2 = \frac{\rho_B U_B^2}{\rho_1 U_1^2}\,\theta_B D_B \quad (23)$$

In order to study the flow field, the governing differential equations for a laminar axisymmetric high-speed wake are transformed from physical coordinates (x,r) to Dorodnitzyn coordinates (x,η), which are related by

$$\eta\, d\eta = \frac{1}{\Delta^2}\,\frac{\rho}{\rho_1}\, r\, dr \tag{24}$$

where

$$\Delta^2 = 2\int_0^{\delta} \frac{\rho}{\rho_1}\, r\, dr \tag{25}$$

The velocity profile in the viscous wake can be assumed to be a fourth order polynomial in η, as

$$\frac{u}{u_1} = a_0 + a_1\eta + a_2\eta^2 + a_3\eta^3 + a_4\eta^4 \tag{26}$$

To determine the coefficients in Eqn 26, the following boundary conditions may be imposed:

At the centerline $\eta = 0$

(1) $u = u_{cl}$

(2) $\dfrac{\partial u}{\partial \eta} = 0$ (27)

(3) axial direction momentum equation applies

At the outer edge of the wake $\eta = 1$

(4) $u = u_1$

(5) $\dfrac{\partial u}{\partial \eta} = 0$ (28)

(6) $\dfrac{\partial^2 u}{\partial \eta^2} = 0$

The above six boundary conditions are needed to determine six unknowns, namely a_0 to a_4, and u_{cl}, provided the flow properties at the outer edge of viscous wake are known from the inviscid wake solution. Applying the above boundary conditions, the velocity profile in the transformed plane becomes

$$\frac{u}{u_1} = 1 - \frac{5}{24}\left(1 - 6\eta^2 + 8\eta^3 - 3\eta^4\right) \tag{29}$$

where

$$\xi = \frac{u_{cl}}{u_1} \Delta^2 \frac{\rho_1}{\mu_{cl}} \frac{du_{cl}}{dx} \tag{30}$$

and also

$$\xi = 24 \left(1 - \frac{u_{cl}}{u_1}\right) \tag{31}$$

It should be noted that:

(1). at the wake stagnation point
$X = 0, \xi = 24, u_{c1} = 0$

(2) at the wake neck $\frac{d\Delta}{dx} = 0, \xi = 22.9$
$\frac{u_{cl}}{u_1} = 0.045$ (32)

(3) far downstream, $X \to \infty$, $\xi = 0$,
$\frac{u_{cl}}{u_1} = 1$

In order to specify the velocity profile completely at any location from the base of forebody, it is necessary to know the distance of the wake stagnation point x_0, from the nose of the forebody, and the relation between ξ, the form parameter, and X, the longitudinal distance from the wake stagnation point. It is difficult to predict the location of a wake stagnation point from mathematical analysis, however, from the limited number of experiments for turbulent flow, it is taken, in Ref 1, that the wake stagnation point is located approximately at 0.94 D_B from the base of the forebody. The relation between ξ and X will then be obtained from Eqn 30. Because of the presence of the viscosity coefficient μ_{cl} in Eqn 30, the relation between ξ and X depends on the laminar or turbulent nature of the flow in the wake. These are discussed in IIB4a(1) and IIB4a(2).

The assumption of zero pressure gradient in the wake and a Prandtl number of unity, leads to a solution of the energy equation in the form

$$\frac{h_{o_1} - h_o}{h_{o_1} - h_{o_{cl}}} = \frac{1 - \frac{u}{u_1}}{1 - \frac{u_{cl}}{u_1}} \tag{33}$$

The total enthalpy, h_{oc1}, at the wake centerline can be determined using the condition that the total enthalpy defect in the wake is constant and is equal to the value at the base of the forebody. Carrying out the algebra, it can be shown that

$$\frac{h_{oc_2}}{h_{o_1}} = 1 - \frac{u_1}{u_B}\left(1 - \frac{h_B}{h_{c_1}}\right)\left(1 - \frac{u_{c_2}}{u_1}\right) \tag{34}$$

where h_B is the enthalpy based on the skin temperature of the forebody at the base. Substituting for h_{oc1} from Eqn 34 and into Eqn 33, we get the total enthalpy profile

$$\frac{h_{c_1} - h_o}{h_{o_1}} = \frac{u_1}{u_B}\left(1 - \frac{h_B}{h_{o_1}}\right)\left(1 - \frac{u}{u_1}\right) \tag{35}$$

Knowing the velocity profile from Eqn 29 and the total enthalpy profile from Eqn 35, the static enthalpy profile can be obtained from the relation

$$h = h_o - \frac{u^2}{2} \tag{36}$$

The assumption of wake static pressure equal to freestream static pressure and the velocity and static enthalpy profiles as determined from 29 and 36 are sufficient to determine all the flow properties in the viscous wake. Since the profiles are determined in terms of Dorodnitzyn coordinate η, it is then necessary to transform back into physical coordinates, using the relation

$$\frac{r^2}{\Delta^2} = 2\int_0^{\eta} \frac{\rho_1}{\rho}\,\eta\,d\eta \tag{37}$$

(1.) Laminar Viscous Wake

In order to specify the velocity and total enthalpy profiles at any specified distance from the base of the forebody, it is necessary to determine the relation between ζ, the form parameter, and X, the longitudinal distance from wake stagnation point. For a laminar flow case, a linear relationship between viscosity and flow field temperature can be assumed (i.e., μ/RT = constant). Because of the validity of the boundary layer assumptions in the viscous wake, we get from the equation of state,

$$\frac{\rho_1}{\mu_{c_2}} = \frac{\rho_{\infty}}{\mu_1} \tag{38}$$

The density at the centerline of wake is given by

$$\rho_e = \frac{\gamma}{\gamma-1}\,\frac{p}{h_e} \tag{39}$$

From the definition of the momentum equation in transformed coordinates,

$$\frac{\theta_1^2}{\Delta^2} = 2\int_0^1 \frac{u}{u_1}\left(1-\frac{u}{u_1}\right)\eta\, d\eta \tag{40}$$

Substituting the velocity profile from Eqn 29 into 40, we get the relationship between Δ, the wake thickness, and ξ, the form parameter.

$$\frac{\theta_1^2}{\Delta^2} \simeq \frac{\xi}{120} - \frac{\xi^3}{5500} \tag{41}$$

Using Eqns 38, 39, 41, 36, 31, and 30, we get a first order non-linear differential equation

$$\frac{d\xi}{dx} = -\frac{\gamma}{\gamma-1}\,\frac{\rho_1}{\mu_1}\,\theta_1^2\,\frac{u_1}{24}\left(1-\frac{\xi}{24}\right)\left(\frac{\xi^2}{120}-\frac{\xi^3}{5500}\right)$$
$$\left[h_{o_1} - h_{o_1}\frac{\xi}{24}\,\frac{u_1}{u_B}\left(1-\frac{h_B}{h_{o_1}}\right) - \frac{u_1^2}{2}\left(1-\frac{\xi}{24}\right)^2\right] \tag{42}$$

Integrating Eqn 42 from $X = 0, \xi = 24$, we get the relationship between ξ and X for a laminar viscous wake:

$$X = -\frac{\gamma}{\gamma-1}\,\frac{\rho_1\theta_1^2}{24}\int_{24}^{\xi} \frac{\left(1-\frac{\xi}{24}\right)\frac{u_1}{\mu_1}\,d\xi}{\left(\frac{\xi^2}{120}-\frac{\xi^3}{5500}\right)\left[h_{o_1} - \frac{u_1}{u_B}\,\frac{\xi}{24}\,h_{o_1}\left(1-\frac{h_B}{h_{o_1}}\right) - \frac{u_1^2}{2}\left(1-\frac{\xi}{24}\right)^2\right]} \tag{43}$$

(2.) Turbulent Viscous Wake

The presence of eddy viscosity in turbulent flow necessitates the use of an effective viscosity coefficient

in Eqn 30 to determine the relationship between ζ, the form parameter, and X, the longitudinal distance from the wake stagnation point. Four viscosity models have been suggested in Refs 1 and 4, however, the third model, namely

$$\mu_d = k \Delta \rho_1 (u_1 - u_{cl}) \tag{44}$$

with a value of k = 0.005 is found to give the best correlation with their experimental results. Substituting Eqn 44 into 30, replacing u_{c1}/u_1 in terms of ζ, from Eqns 31 and 41, we get a first order ordinary differential equation in the form (for the third viscosity model)

$$\frac{d\zeta}{d\tilde{x}} = -\frac{k}{\theta_1} \frac{\zeta^2}{\left(1 - \frac{\zeta}{24}\right)} \sqrt{\frac{\zeta^2}{120} - \frac{\zeta^3}{5500}} \tag{45}$$

Assuming the wake momentum thickness, θ_1, to be a constant, and integrating Eqn 45 from X_{TR}, the turbulent wake transition location, we get the relationship between ζ and X as

$$\frac{k}{\theta_1}(X - X_{TR}) = \left(\frac{80}{\zeta^2} - \frac{6.5}{\zeta}\right)\sqrt{\frac{\zeta}{120} - \frac{\zeta^2}{5500}} \Bigg|_{\zeta_{TR}}^{\zeta} \tag{46}$$

where X_{TR} = location of wake transition point and $\zeta_{TR} = \zeta$ laminar at transition point.

Similarly, the relationship between ζ and X can be obtained for other viscosity models, but in a more complicated form. If the flow on the forebody surface is turbulent, then $X_{TR} = 0$. If the flow is completely laminar on the forebody surface, it may be laminar or turbulent in the wake. A wake transition criterion, discussed in IIB4a(3), must be used to determine the location of the transition point, X_{TR}.

(3.) Wake Transition Criterion

The location of the wake transition point X_{TR} from laminar to turbulent wake flow can be determined primarily by using available experimental data. In Ref 1, an approximate curve fit correlating experimental results of Pallone, Erdos, and Eckerman (Ref 5) has been used as the wake transition criterion. The wake transition Reynolds number $Re_{\delta_{DTR}}$ is based on viscous wake properties at the edge of the wake with

the relative velocity between the centerline velocity and velocity at wake edge as

$$Re_{\delta_{OTR}} = \frac{\rho_1 (u_1 - u_\alpha)\delta_{OTR}}{\mu_1} \tag{47}$$

and effective Mach number is defined as

$$\overline{M_1} = \frac{u_1 - u_\alpha}{a_1} \tag{48}$$

At the transition point, transition Reynold's number and effective Mach Number $\overline{M_1}$ are related (according to a curve fit in Ref 1) by

$$Re_{\delta_{OTR}} = 1700\ \overline{M_1}^{2.2} \tag{49}$$

If the flow on the forebody surface is completely laminar, the laminar viscous wake analysis of IIB4a(1) is continued until the wake transition criterion (49) is satisfied. The point X_{TR} and the value $\rho_{laminar}$ at this point are used in continuing the turbulent wake analysis of IIB4a(2).

b. Inviscid Wake

The inviscid wake analysis essentially determines the flow properties beyond the viscous wake edge at any specified location behind the base of the forebody. The following assumptions have been made in the far wake region.

1. The secondary shocks, such as the wake recompression shocks, forebody flare shocks, if any, are considered to be very weak so that they produce negligible change in entropy.

2. There is no radial pressure gradient $\frac{dp}{dr}$ in the wake.

3. In the far wake region static pressure in the wake approaches the freestream static pressure.

The inviscid wake depends mainly on the shape and strength of forebody shock. The total pressure, total temperature and entropy at any radius r from the axis of wake are equal to the corresponding values at radius r_s immediately behind the forebody shock. Since the forebody

shock is completely specified, flow properties immediately behind the shock are given by shock jump conditions. The relation between r and r_s is given by the conservation of mass,

$$r_s^2 = 2\int_{\delta^*}^{r} \frac{\rho u}{\rho_\infty u_\infty} r\,dr \tag{50}$$

where the integration in Eqn 50 is started from δ^*, the wake displacement thickness, to take into account the displacement of streamlines. The wake displacement thickness δ^*, is defined by

$$\delta^* = 2\int_0^{\delta}\left(1 - \frac{\rho u}{\rho_1 u_1}\right) r\,dr \tag{51}$$

To facilitate the computation (X, r) coordinates are transformed into (X, n) where

$$\rho u r\,dr = \rho_\infty u_\infty n\,dn \tag{52}$$

So that Eqn 50 becomes

$$r_s^2 = n^2 - \frac{\rho_1 u_1}{\rho_\infty u_\infty^*}\delta^{*2} \tag{53}$$

In order to transform back into physical coordinates, r and n are related by

$$r^2 - \delta^{*2} = 2\int_{\sqrt{\frac{\rho_1 u_1}{\rho_\infty u_\infty}}\delta^*}^{n} \frac{\rho_\infty u_\infty}{\rho u} n\,dn \tag{54}$$

The computational procedure is as follows:

1. From the results of the viscous wake analysis, the wake displacement thickness δ^* can be calculated from Eqn 51.

2. For any transformed radius n, Eqn 53 is used to find r_s.

3. Total pressure, total enthalpy and entropy at the transformed radius n are the same as that at radius r_s immediately behind the forebody shock.

4. Static pressure is assumed to be equal to freestream static pressure. From total pressure and static pressure the Mach number at transformed radius n can be found using isentropic relations. All other flow properties at this location can then be found.

5. Radial distance r from the axis of symmetry corresponding to transformed radius n can be found using Eqn 54.

6. Since the viscous wake analysis depends on the inviscid solution at the edge of viscous wake, an iteration procedure is adopted to determine the complete wake profile.

C. Assumptions and Validity

1. Forebody Pressure Distribution

The method of predicting the forebody pressure distribution has been discussed in Appendix II of Ref 1. The surface pressure distribution is needed as an input to the boundary layer calculations. The Newtonian method is used if the shock wave is detached from the body and the tangent-cone method is used if the shock wave is attached. These methods of predicting surface pressure distribution can be fairly accurate in many cases, but inaccurate in others. If the error in pressure drag coefficient is chosen as an indicator of the accuracy of these techniques, Fig 17.18b of Ref 6 can be used to estimate the range of applicability of the techniques. From this figure one finds that an error of about ten per cent or less occurs if $M_\infty \tau \geq 1$. M_∞ represents the freestream Mach number and τ represents the thickness ratio of the body under consideration. For the Arapaho C vehicle, (Configuration 2, Fig 2, Ref 7) a thickness ratio of $\tau = 1/8$ is appropriate. Thus, we infer that the surface pressure distribution technique of Ref 1 (for an Arapaho C vehicle) is valid only for freestream Mach numbers in the range $M_\infty \geq 8$. For the modified Arapaho C with a flared afterbody, $\tau = 1/4$ (Configuration 3, Fig 2, Ref 7), the methods are valid for $M_\infty \geq 4$. It should be noted that we have used an integrated pressure distribution (pressure drag coefficient) to determine these ranges of validity. It should be remembered, as pointed out in Ref 6, page 676, that a good agreement in pressure drag coefficient does not imply good agreement in surface pressure distribution.

It is difficult to estimate the errors of the surface pressure prediction method in the prediction of wake properties. However, in many cases it would probably be preferable to utilize the method of characteristics to predict the forebody pressure distribution.

2. Forebody Boundary Layer Calculations

The treatment of the boundary layer growth along the surface of the forebody is based on empirical expressions and relationships that appear to provide a good description of the experimentally observed data. From the standpoint of practical application, it would appear that the boundary layer techniques utilized in Ref 1 are adequate for engineering applications.

3. Viscous Wake Analysis

The assumptions made to arrive at a solution for the viscous wake in Ref 1 (Fig 97) are presented below:

1. The fluid is thermally and calorically perfect, and there are no chemical reactions or other real gas phenomena.

2. Prandtl number is unity (Pr = 1).

3. Prandtl's concept of viscous flow phenomena is valid for the high-speed compressible wake in such a way that gradients in the streamwise or axial direction are much smaller than those normal to the wake axis, and boundary layer type equations can be used.

4. The details of the base flow and free shear can be largely ignored. Thus, the region of validity for the present analysis must be considered to extend from somewhere in the vicinity of the wake neck, or further downstream, down into the far wake.

5. Effects due to the existence of an external pressure gradient are negligible.

These assumptions from the basis of classical boundary layer theory have been the basis for many successful analytical studies. However, assumptions 3 and 5 become increasingly less valid as the base of the forebody is approached.

A further assumption is implied by Eqn 59 of Ref 1, namely, that the velocity profiles in the wake are similar at any axial location. This assumption also becomes increasingly inaccurate as the wake neck region is approached.

It is also assumed in Ref 1, Eqn 54, that the momentum defect in the wake is equal to the momentum defect in the boundary layer at the base of the forebody. Data

presented in Table I of Ref 1 shows that this assumption is not completely valid. However, it may be possible to introduce an empirical factor that relates the boundary layer momentum defect at the base to the far wake momentum defect.

The choice of an appropriate turbulent viscosity model is discussed in Ref 1 and four models are considered. The third model, $\mu_{cl} = k\Delta\delta_1(u_1 - u_{cl})$ with k = 0.005 provided the best correlation with experimental results. It is impossible to say, with only this one body having been considered, that the same viscosity model will be appropriate for all bodies.

It was found that the viscous wake analysis provided agreement with experiment to well within 10 per cent in Ref 1. Considering the number of assumptions employed and the complex phenomena being studied, this is considered to be excellent agreement.

4. Inviscid Wake Analysis

The method used to predict the inviscid wake characteristics in Ref 1 must be considered only as a first order method. The assumption of isentropic flow along streamlines behind the bow shock is valid only for certain configurations where no trailing shock waves have been generated. The method of characteristics could be employed for a second order prediction of the inviscid wake region, but this requires considerably more effort and complexity.

5. Summary

The forebody and wake analysis technique, despite some of its shortcomings, appears to be the best available method for wake predictions. Several improvements and refinements could be made, but the increase in accuracy may not justify a more complext technique.

D. Experimental Comparisons

Using the methods just described, sample calculations were completed for a cone-cylinder body in a supersonic flow with $M_\infty = 2.98$ and a Re/ft of 8.86×10^5. The results of these calculations were checked with wind tunnel experiments conducted at the Rosemount Aeronautical Laboratories, University of Minnesota, at the Supersonic Gasdynamics Facility of the Flight Dynamics Laboratory at Wright-Patterson Air Force Base, and at the Arnold Engineering Development Center's von Karman Gas Dynamics Facility. Figure 2 shows the geometry of the forebody and the two sizes that were tested; calculations were made for the $D_B = 2$ in. forebody. In this section the results of the calculations and experiments are compared.

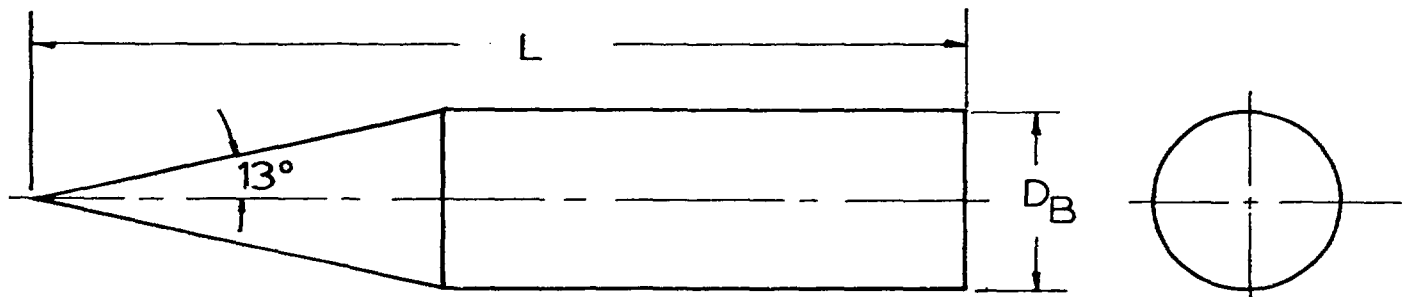

$L/D_B = 6.195$

TEST FACILITIES

$L = 7.428$ in, $D_B = 1.200$ in	U OF M
$L = 12.390$ in, $D_B = 2.00$ in	AFFDL - SGF AEDC - VKF

Fig 2 Geometry of Forebodies used for Experiments

1. Forebody Shock Shape

Although the forebody shock shape is not a result, it is a required input to the method of calculation. Thus the forebody was sting mounted in a Rosemount Aeronautical Laboratory 12 in x 12 in blowdown tunnel and Schlieren photographs obtained (Fig 3). As shown, at M_∞ = 2.98 the shock is attached and nearly conical. From these photographs the shock geometry was determined and used as an input to the calculations.

2. Forebody Surface Pressures

The surface pressures of the forebody are a result of the calculation. These pressures were measured in tests conducted at the AFFDL Supersonic Gasdynamics Facility continuous flow tunnel at M_∞ = 2.98. Figure 4 shows the pressure distribution model installed in the SGF tunnel, and Fig 5 shows the test results and the results of the calculation.

As shown in Fig 5 the results are quite good. As would be expected, the measured surface pressure on the conical portion of the body agrees almost perfectly with the calculated pressure. Downstream of the conical portion the measured pressures are at first lower, then approach the calculated values. This is no doubt due to the inaccurate calculation of the flow expansion occurring at the intersection of the conical and cylindrical portions.

3. Base Momentum Defect

The momentum defect at the base of the body was also measured with small boundary layer probes in the tests at the AFFDL SGF tunnel (Fig 6). Figure 7 shows the velocity profile results from these measurements and Table I compares the results of these measurements with the calculation. There is a 23% difference in these values, which is probably consistent with the accuracy of the assumptions made in the boundary layer analysis.

4. Wake Characteristics

Figures 8 through 13 show comparisons of measured and calculated wake characteristics. The measured values presented here have been obtained from Ref 8. These tests were conducted at M_∞ = 2.98 in an Arnold Engineering Development Center continuous flow tunnel. One sees from the figures that there is a considerable difference in the results, due primarily to the fact that the measured wake is considerably thicker than the calculated wake. Other than this, the general trends are similar and the wake centerline and edge values are in reasonable agreement. This

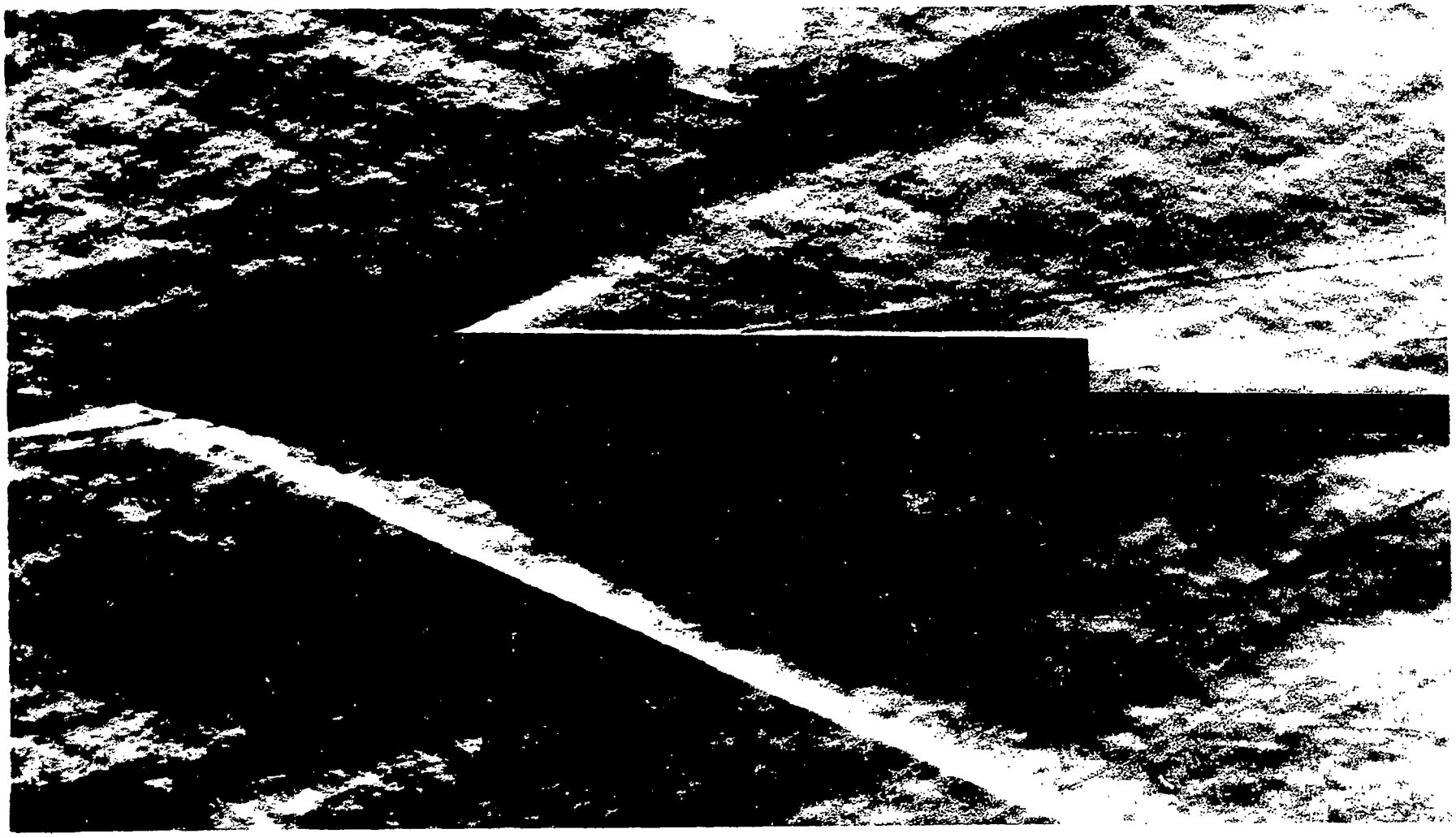

Fig 3 Forebody Shock Shape, Sting Mounted, $M_\infty = 2.98$

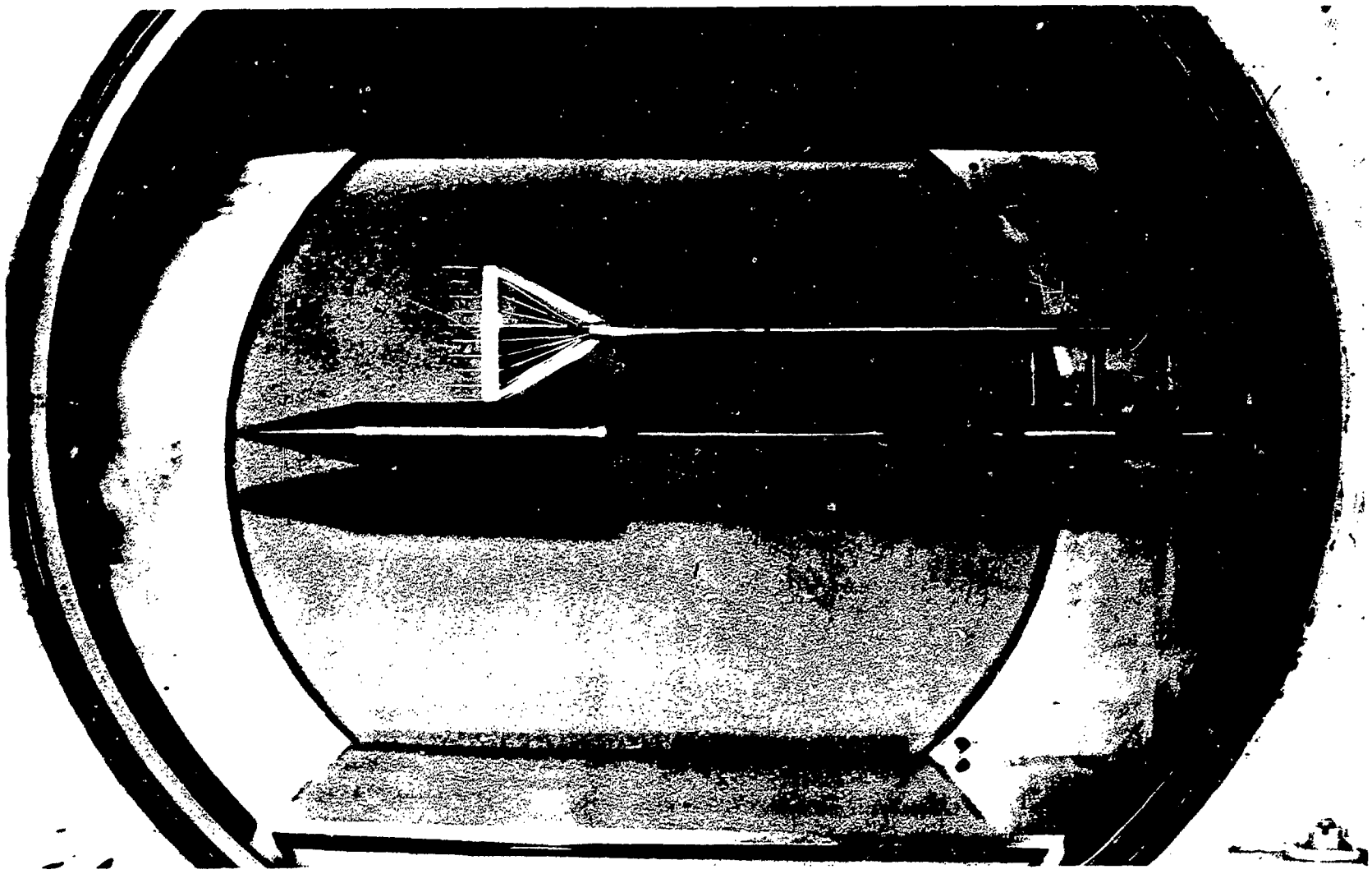

Fig 4 Forebody Pressure Distribution Model, Sting Mounted, $M_\infty = 2.98$

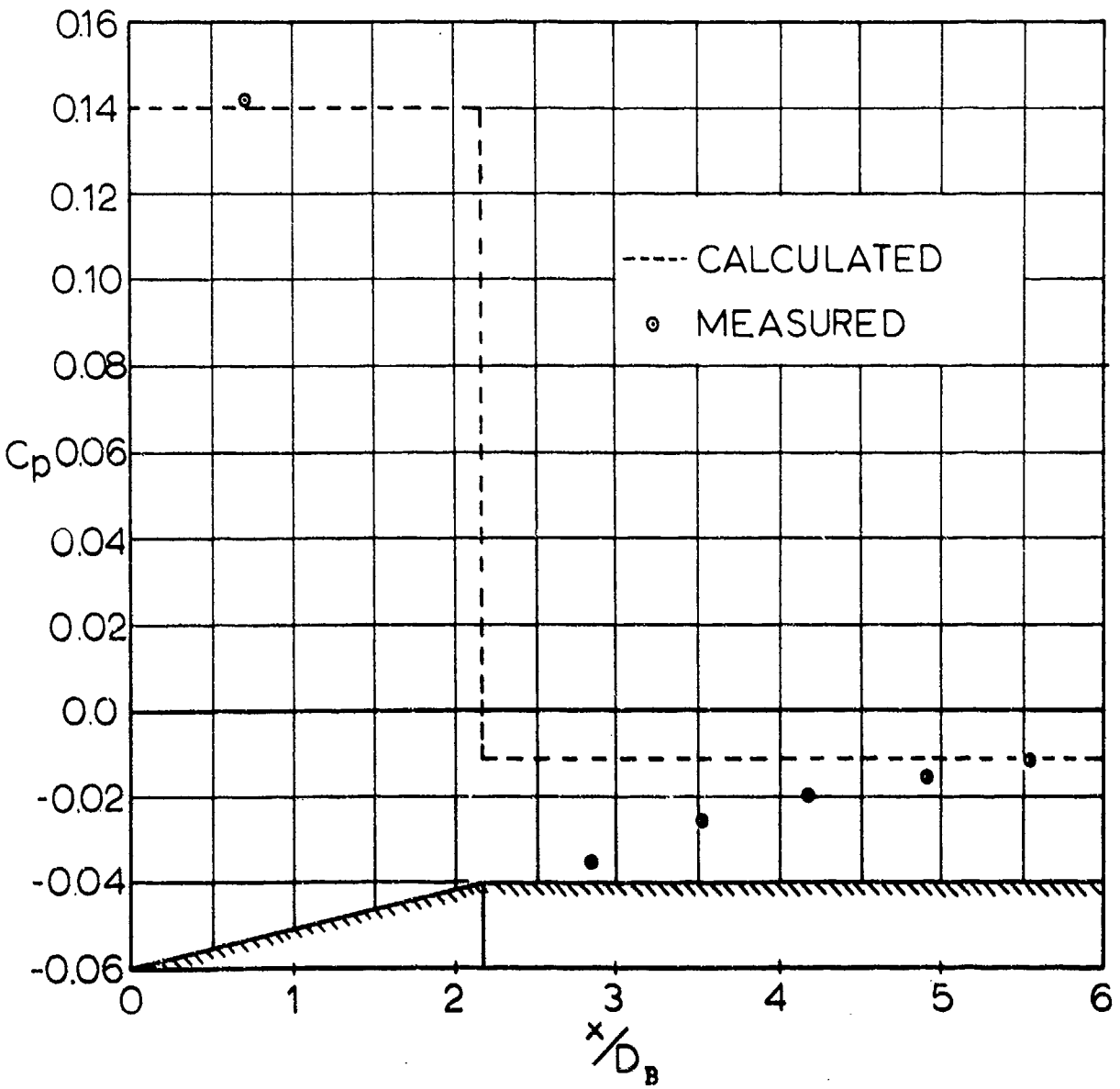

Fig 5 Comparison of Measured and Calculated Forebody Surface Pressures $M_\infty = 2.98$ $Re_\infty = 9.3362 \times 10^5$

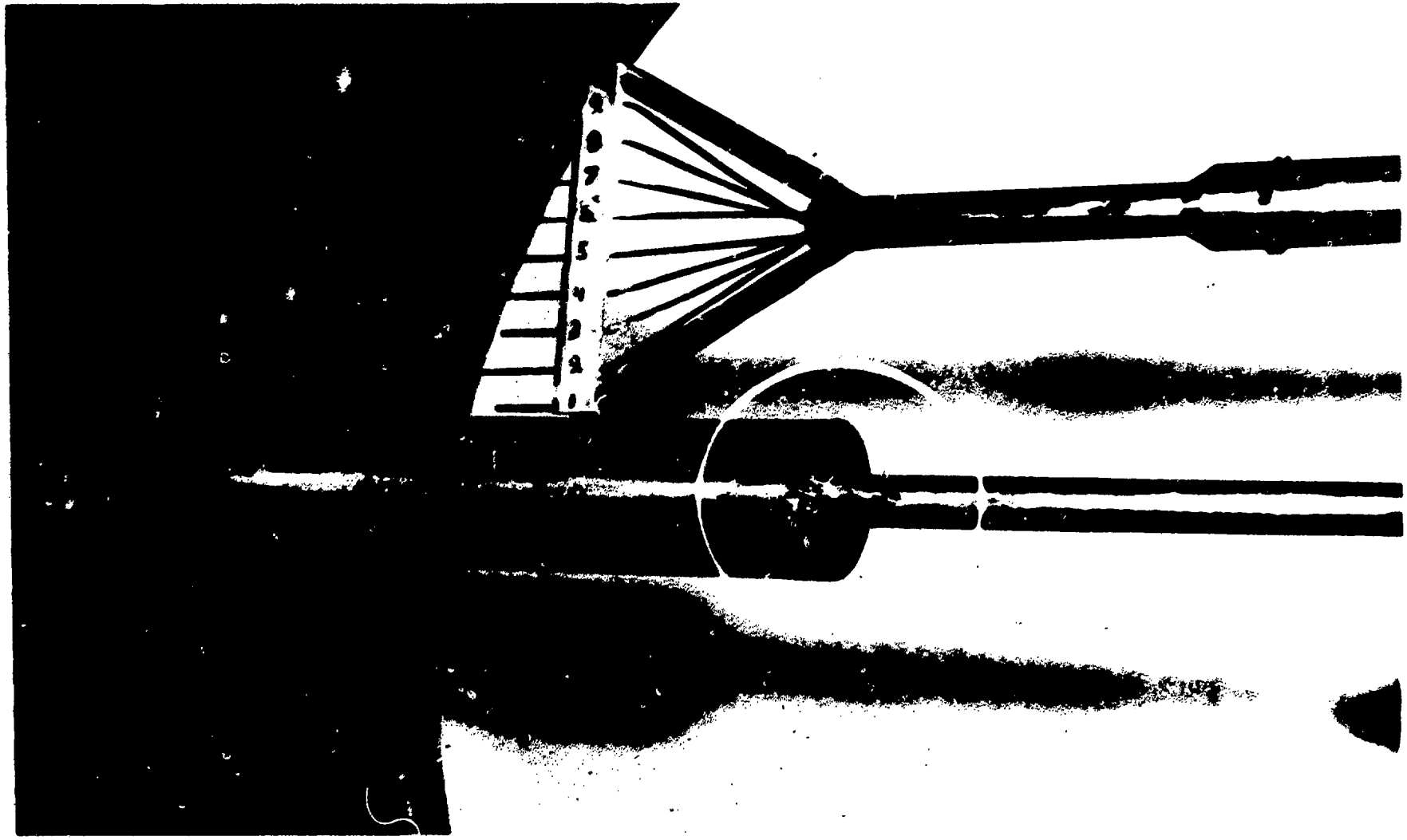

Fig 6 Forebody Base Momentum Defect Measurement, Boundary Layer Probes, $M_\infty = 2.98$

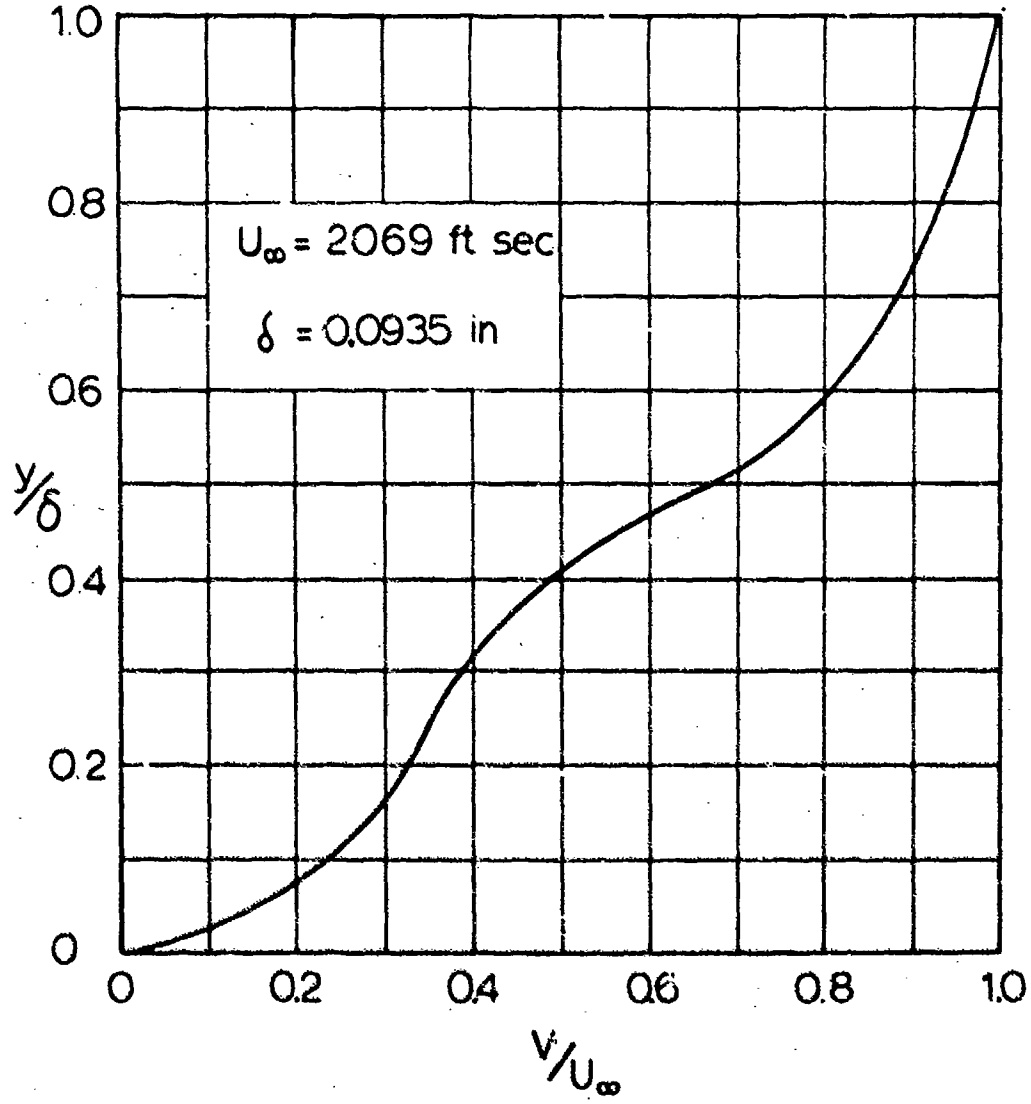

Fig 7 Velocity Profiles in the Boundary Layer of the Forebody at its Base M_∞=2.98 $Re_{/ft} = 8.874 \times 10^4$

TABLE I

MOMENTUM DEFECT AT THE FOREBODY BASE AND IN THE WAKE ($M_\infty = 2.98$, REYNOLDS NO/FT $= 8.855 \times 10^5$)

Location	Momentum Defect (lb)	
	Experimental	Theory
Base	0.081	0.062
$1/D_B = 5$	0.314	0.062
$1/D_B = 7$	0.336	0.062
$1/D_B = 9$	0.311	0.062

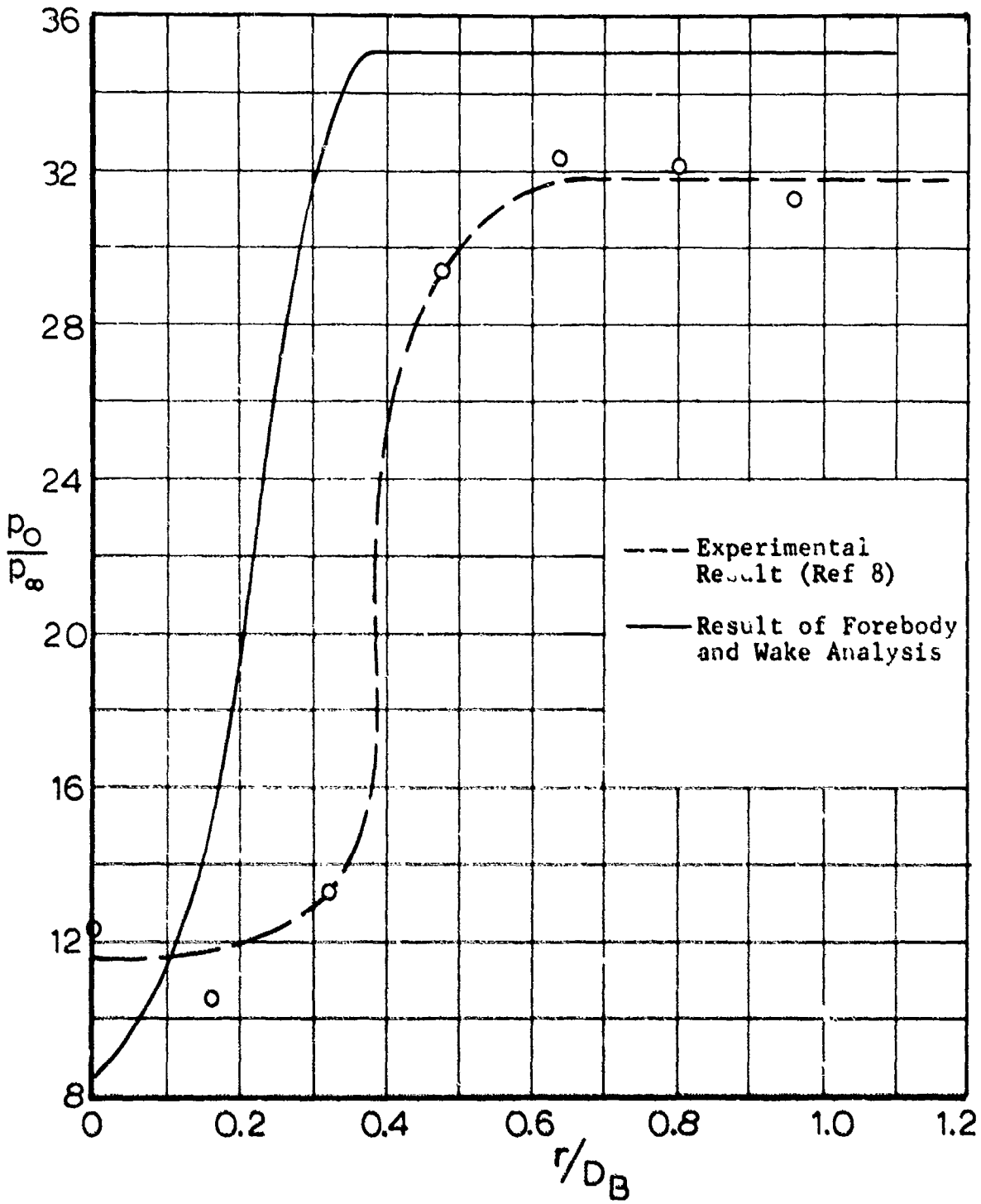

Fig 8 Wake Total Pressure Distribution
$M_\infty = 2.98$, $\ell/D_B = 5.0$

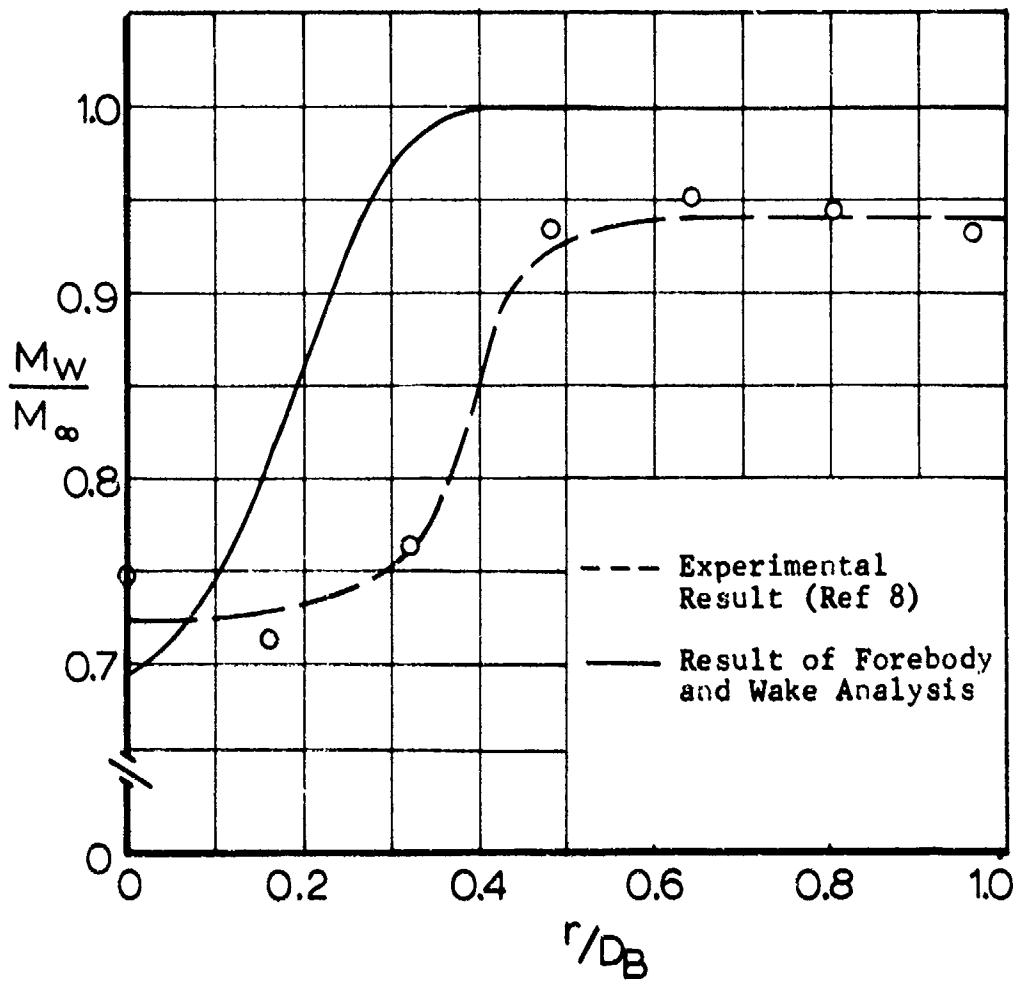

Fig 9 Wake Mach Number Distribution
$M_\infty = 2.98$, $\ell/D_B = 5.0$

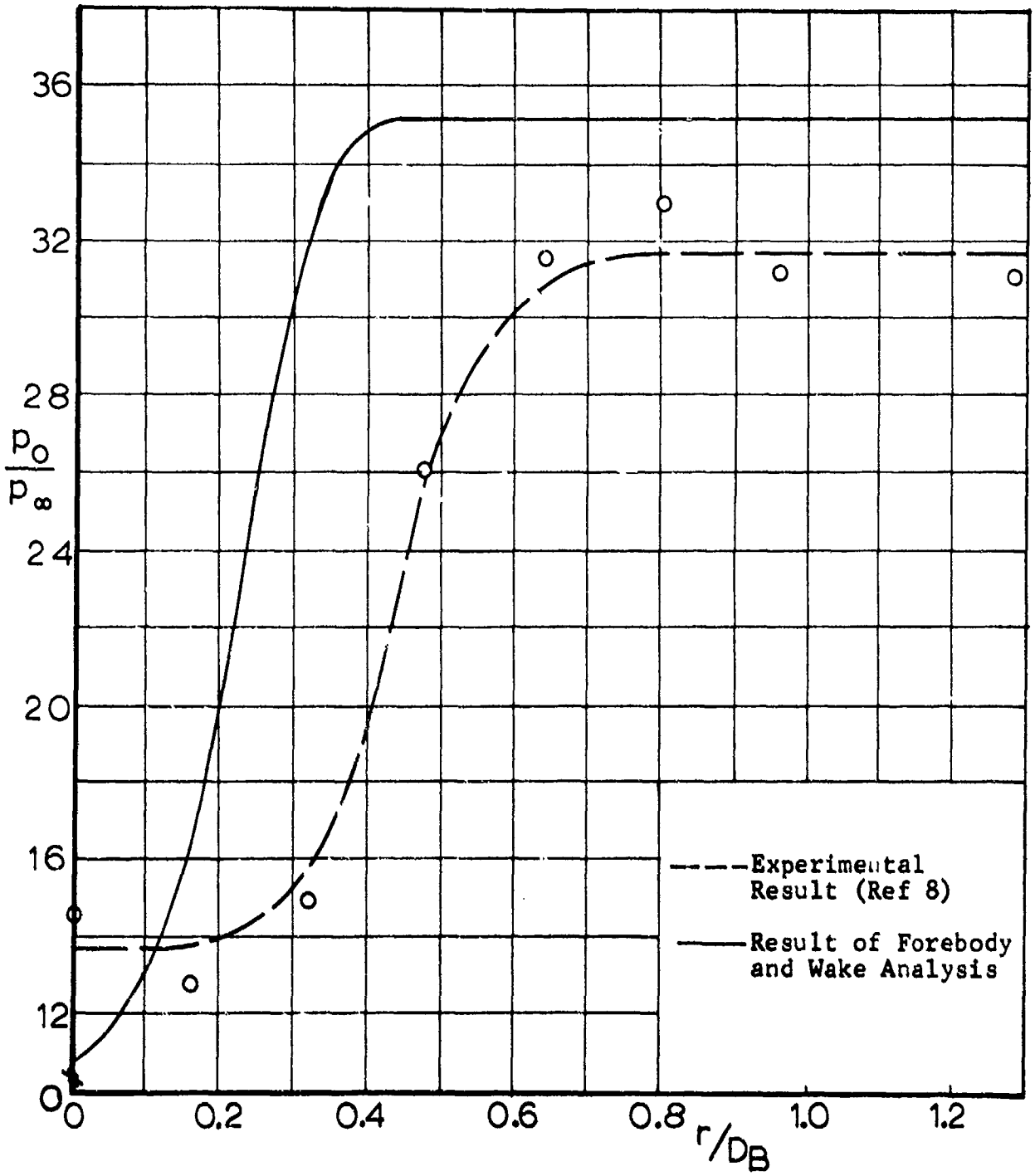

Fig 10 Wake Total Pressure Distribution
$M_\infty = 2.98$, $\ell/D_B = 7.0$

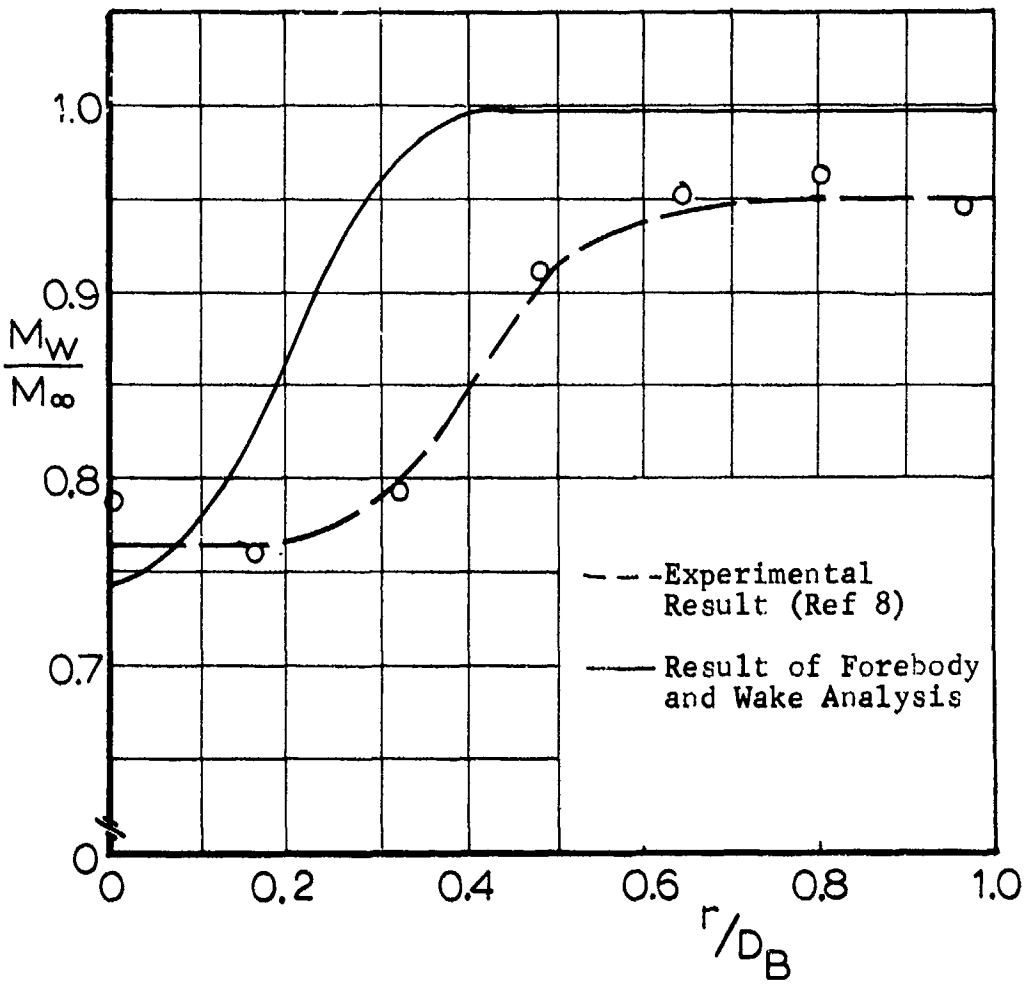

Fig 11 Wake Mach Number Distribution
$M_\infty = 2.98$, $\ell/D_B = 7.0$

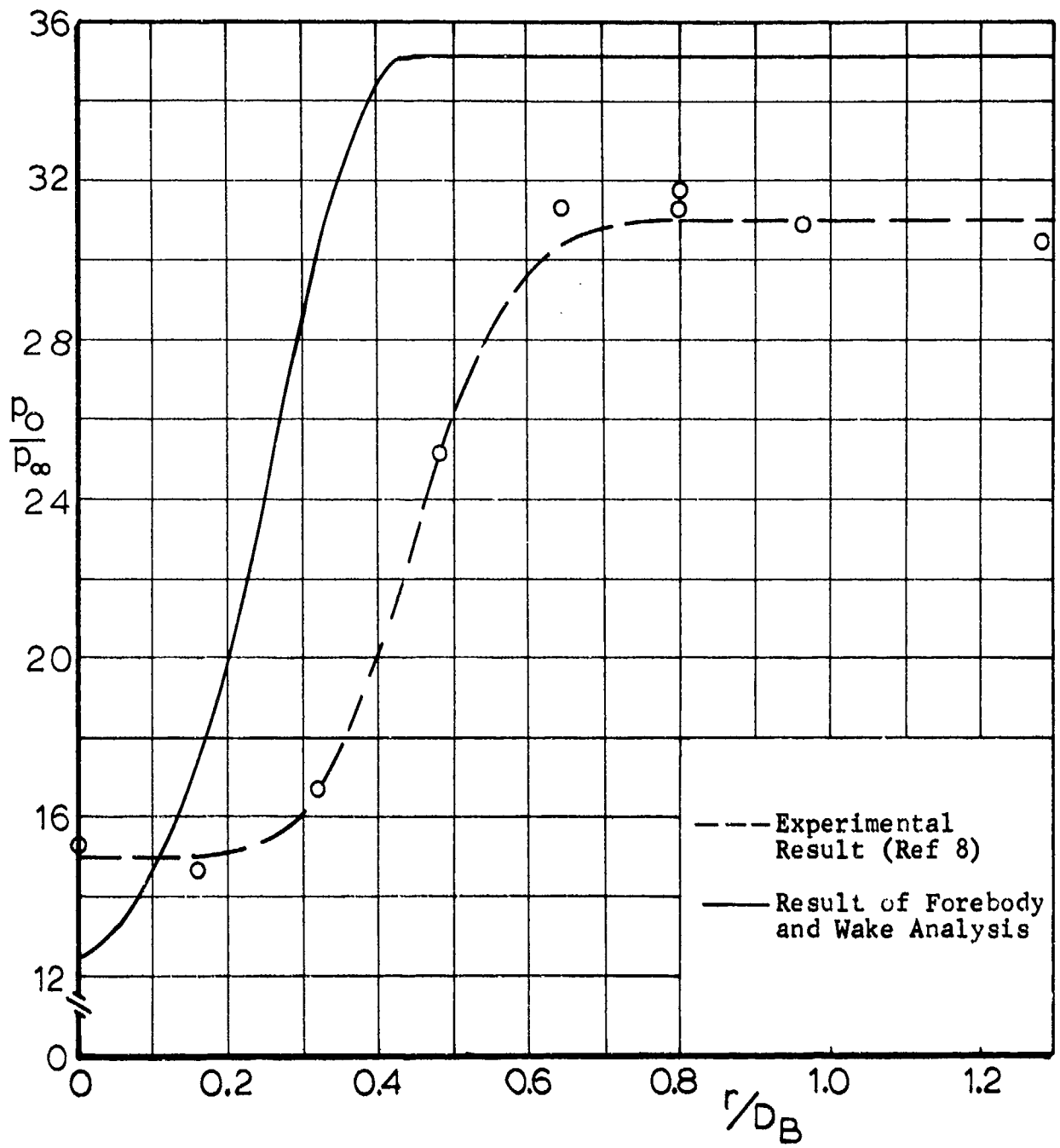

Fig 12 Wake Total Pressure Distribution
$M_\infty = 2.98$, $\ell/D_B = 9.0$

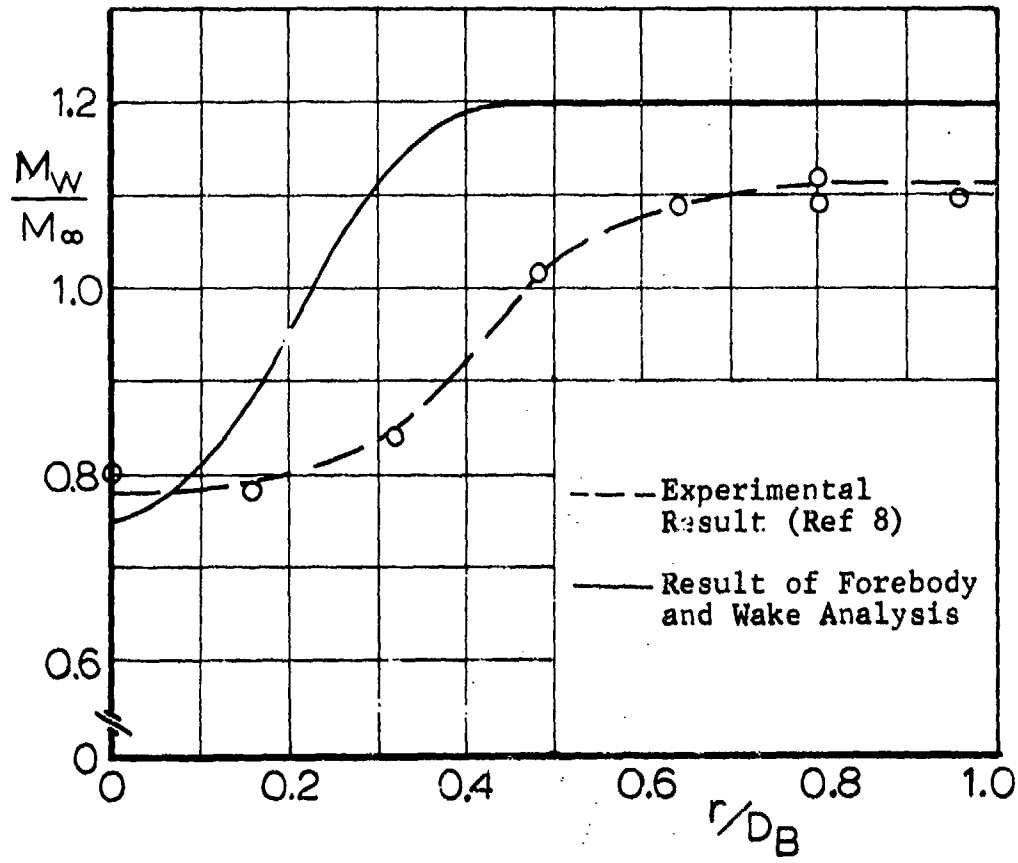

Fig 13 Wake Mach Number Distribution
$M_\infty = 2.98$, $\ell/D_B = 9.0$

discrepancy in wake width could be lessened by adjusting some of the coefficients used in the wake analysis, but time did not allow this effort.

III. SECONDARY BODY ANALYSIS

In view of the over-all objectives of this study, once the analysis of the primary body had been completed, the next effort was directed at the secondary body, the decelerator. Analytical techniques have been developed for predicting the flow field properties about certain classes of secondary bodies using the method of characteristics. This section explains the theory of the method used and compares its results with measurements; details of the actual calculations are described in Vol II of this report.

A. Extent of the Secondary Body Analysis, Required Inputs, and Results

1. Extent of the Analysis

The analysis used for the secondary body extends axially from the upstream tip of the secondary body downstream to the base of the body. The wake of the secondary body is not included in the analysis. Normal to the axis of symmetry, the analysis extends from the secondary body surface to its bow shock wave; flow field characteristics outside of the bow shock can be obtained from the wake analysis of the forebody.

2. Required Inputs

The information required for the secondary body analysis includes the upstream flow properties, the pressure and temperature distributions, and the geometry of the body. The computer program discussed in Vol II is such that the upstream flow conditions can either be calculated using the primary body analysis or an input to the program. In order to obtain a pressure drag coefficient the base pressure of the body must be obtained.

3. Results of the Analysis

The method calculates all the flow properties from the body surface to the shock wave. Thus the shock shape, surface pressures, and pressure drag are obtained.

B. Explanation of the Method Used for the Secondary Body Analysis

1. Theory

In order to predict the flow field surrounding an aerodynamic decelerator in the wake of a forebody, several

assumptions and restrictions have been made.

1. The flow is inviscid and steady
2. The gas is thermally and calorically perfect.
3. The flow is supersonic everywhere in the region of interest.
4. The wake flow field is known, either from theory or experiment.

The first three assumptions permit one to develop a method of characteristics for rotational, non-homoenergic flow. The fourth assumption establishes an effective "upstream" boundary condition for the problem.

The basic equations under the above assumptions are as follows:

Continuity equation,

$$\nabla \cdot \rho \vec{V} = 0 \tag{55}$$

Momentum equation,

$$\rho (\vec{V} \cdot \nabla) \vec{V} = -\nabla p \tag{56}$$

First Law of Thermodynamics,

$$\nabla h = T \nabla S + \frac{1}{\rho} \nabla p \tag{57}$$

Using the vector identity

$$(\vec{V} \cdot \nabla)\vec{V} = -\vec{V} \times (\nabla \times \vec{V}) + \nabla \frac{V^2}{2} \tag{58}$$

Equation 56 can be written as

$$-\vec{V} \times \vec{\omega} + \nabla \frac{V^2}{2} = -\frac{\nabla p}{\rho} \tag{59}$$

where $\vec{\omega}$ represents the vorticity and is defined by

$$\vec{\omega} = \nabla \times \vec{V} \tag{60}$$

Solving Eqn 57 for $\frac{1}{\rho}\nabla p$ and substituting into Eqn 59 yields a convenient form of the momentum equation

$$\vec{V} \times \vec{\omega} = -T\nabla S + \nabla\left(h + \frac{V^2}{2}\right) \tag{61}$$

If one takes the dot product of the velocity $\vec{V}$ with Eqn 61, there results

$$-T\,\vec{V}\cdot\nabla S + \vec{V}\cdot\nabla\left(h + \tfrac{1}{2}V^2\right) = 0 \tag{62}$$

If one assumes that the total energy is constant along a streamline, then Eqn 62 shows that the entropy is also constant along a streamline.

Taking the dot product of Eqn 61 with a unit normal vector to the streamline, $\hat{n}$, one obtains

$$\hat{n}\cdot(\vec{V}\times\vec{\omega}) = -T\frac{dS}{dn} + \frac{dh_o}{dn} \tag{63}$$

where $h_o = h + \frac{V^2}{2}$ = total enthalpy. (64)

The vorticity, in cylindrical coordinates, can be written as

$$\vec{\omega} = \nabla\times\vec{V} = \left(\frac{\partial v}{\partial x} - \frac{\partial u}{\partial r}\right)\hat{k} \tag{65}$$

It can be shown that, for axially symmetric flow, the unit normal vector is given by

$$\hat{n} = -\frac{v}{V}\hat{i} + \frac{u}{V}\hat{j} \tag{66}$$

One can then evaluate the left side of Eqn 63 to obtain

$$\left[\frac{\partial u}{\partial r} - \frac{\partial v}{\partial x}\right]V = -T\frac{dS}{dn} + \frac{dh_o}{dn} \tag{67}$$

Using conventional relationships between local static and total properties (Ref 2), it can be shown that the density and speed of sound are given by

$$\rho = 2\frac{\gamma}{\gamma-1}\frac{p_o}{(2h_o)^{\frac{2\gamma}{\gamma-1}}}\left[2h_o - V^2\right]^{\frac{1}{\gamma-1}} \tag{68}$$

$$a^2 = \frac{\gamma-1}{2}\left[2h_o - V^2\right] \tag{69}$$

Substituting Eqn 68 into the continuity equation 55 gives

$$\nabla\cdot\left[\frac{p_o}{(2h_o)^{\frac{2\gamma}{\gamma-1}}}(2h_o - V^2)^{\frac{1}{\gamma-1}}\vec{V}\right] = 0 \tag{70}$$

which may be expanded to

$$\nabla\left[\frac{p_o}{(2h_o)^{\frac{2\gamma}{\gamma-1}}}\right]\cdot\left[(2h_o - V^2)^{\frac{1}{\gamma-1}}\vec{V}\right] + \frac{p_o}{(2h_o)^{\frac{2\gamma}{\gamma-1}}}\nabla\cdot\left[(2h_o - V^2)^{\frac{1}{\gamma-1}}\vec{V}\right] = 0 \tag{71}$$

Since total pressure (p_o) and enthalpy (h_o) have been shown to be constant along a streamline, one can write

$$\vec{V}\cdot\nabla\left[\frac{p_o}{(2h_o)^{\frac{2\gamma}{\gamma-1}}}\right] = 0 \tag{72}$$

and Eqn 71 becomes

$$\nabla\cdot\left[(2h_o - V^2)^{\frac{1}{\gamma-1}}\vec{V}\right] = 0 \tag{73}$$

In cylindrical coordinates, this can be expressed as

$$\frac{\partial}{\partial x}\left[r(2h_o - v^2)^{\frac{1}{\gamma-1}} u\right] + \frac{\partial}{\partial r}\left[r(2h_o - v^2)^{\frac{1}{\gamma-1}} v\right] = 0 \qquad (74)$$

This relation implies the existence of a stream function that satisfies the relations

$$u = \frac{1}{r}\left[2h_o - v^2\right]^{-\frac{1}{\gamma-1}} \frac{\partial \psi}{\partial r} \qquad (75)$$

$$v = -\frac{1}{r}\left[2h_o - v^2\right]^{-\frac{1}{\gamma-1}} \frac{\partial \psi}{\partial x} \qquad (76)$$

A characteristic equation, involving the stream function, can be developed from Eqn 67 in the following fashion. As a convenient shorthand notation, we will indicate partial differentiation of a variable with a subscript. Thus, for example,

$$\frac{\partial \psi}{\partial x} = \psi_x \qquad (77)$$

$$\frac{\partial^2 \psi}{\partial x \partial r} = \psi_{xr} \qquad (78)$$

If we let

$$f = \frac{\left[2h_o - v^2\right]^{-\frac{1}{\gamma-1}}}{r} \qquad (79)$$

Eqns 75 and 76 can be written

$$u = f\psi_r \qquad (80)$$

$$v = -f\psi_x \qquad (81)$$

Using these relations, the bracketed portion on the left side of Eqn 67 can be written

$$u_r - v_x = (\psi_{xx} + \psi_{rr}) f + (f_r \psi_r + f_x \psi_x) \tag{82}$$

By squaring Eqns 80 and 81 and adding the results, one obtains

$$\psi_x^2 + \psi_r^2 = \frac{V^2}{f^2} \tag{83}$$

Taking the gradient of Eqn 83 gives

$$2 \psi_x \nabla \psi_x + 2 \psi_r \nabla \psi_r = \nabla \left(\frac{V^2}{f^2} \right) \tag{84}$$

Taking the dot product of $\hat{n}$, Eqn 66 with Eqn 84 results in

$$\frac{v^2}{fV} \psi_{xx} - \frac{2uv}{fV} \psi_{xr} + \frac{u^2}{fV} \psi_{rr} = \frac{\hat{n} \cdot \nabla \left(\frac{V^2}{f^2} \right)}{2} \tag{85}$$

One can rearrange Eqn 79 to obtain

$$\frac{V^2}{f^2} = 2 h_o f^{-2} - r^{(1-\gamma)} f^{-(\gamma+1)} \tag{86}$$

Using this relation, the right side of Eqn 80 can be evaluated. After considerable algebraic manipulations, Eqn 85 is transformed to the following

$$\psi_x f_x + \psi_r f_r = -v^2 f \psi_{xx} + 2uvf \psi_{xr} - u^2 f \psi_{rr} + \frac{\frac{\gamma-1}{2} r^{-\gamma} f^{-\gamma+2} \psi_r + v \frac{dh_o}{dn}}{V^2 - a^2} \tag{87}$$

Substituting Eqn 87 into Eqn 78 provides, after algebraic manipulation

$$u_r - v_x = \left[(u^2 - a^2)\,\psi_{xx} + (v^2 - a^2)\,\psi_{rr} + 2uv\,\psi_{xr} + \right.$$

$$\left. + \frac{\gamma - 1}{2}\, r^{-\gamma+1} f^{-\gamma+1} \frac{\psi_r}{r} + \frac{V}{f} \frac{dh_o}{dn} \right] \frac{f}{V^2 - a^2} \qquad (88)$$

Substitution of Eqn 88 into Eqn 67 provides the final equation

$$\left[1 - \frac{u^2}{a^2}\right] \psi_{xx} + \left[1 - \frac{v^2}{a^2}\right] \psi_{rr} - 2\,\frac{uv}{a^2}\,\psi_{xr} - \frac{\psi_r}{r} =$$

$$= \frac{r}{V} \left[2h_o - V^2\right]^{\frac{1}{\gamma-1}} \frac{dh_o}{dn} - \frac{\gamma - 1}{2\gamma} \frac{r}{V} \left[2h_o - V^2\right]^{\frac{\gamma}{\gamma-1}} \left[1 - \frac{V^2}{a^2}\right] \frac{dS/R}{dn} \qquad (89)$$

The equation for the stream function is identical to Eqn 9.65 of Ref 6 with the exception of the terms on the right side of Eqn 89. Equation 9.65 of Ref 6 was derived for irrotational flow. Thus, the terms on the right side of Eqn 89 describe the effect of entropy and enthalpy gradients on the flow field.

The general theory of characteristics is presented and discussed in Appendix A of Ref 6. A characteristic curve is one on which ψ_x and ψ_r are discontinuous. If we write Eqn 89 in the form

$$A\,\psi_{xx} + 2B\,\psi_{xr} + C\,\psi_{rr} = D \qquad (90)$$

it can be shown that the slope, λ, of the characteristic curves is given by

$$\lambda = \frac{dr}{dx} = \frac{B \pm \sqrt{B^2 - AC}}{A} \qquad (91)$$

As shown in Ref 6, page 484, this relation reduces to

$$\lambda \equiv \frac{dr}{dx} = \tan(\theta \pm \mu) \tag{92}$$

where μ is the Mach angle given by

$$\sin\mu = \frac{1}{M} \tag{93}$$

Since $\sin\mu$ is defined only for $M \geq 1$, one notes an important feature of the method of characteristics, namely, it can be used only in regions where the flow field is supersonic.

We now proceed to establish the equation describing the variation of the stream function along the characteristic curves. In general, one may write

$$d\psi_x = \psi_{xx}\,dx + \psi_{xr}\,dr = \left[\psi_{xx} + \psi_{xr}\frac{dr}{dx}\right]dx \tag{94}$$

On a characteristic curve, Eqn 94 can be written

$$\left(\frac{d\psi_x}{dx}\right)_{char} = \psi_{xx} + \lambda\psi_{xr} \tag{95}$$

which can be rearranged to give

$$\psi_{xx} = \left(\frac{d\psi_x}{dx}\right)_{char} - \lambda\psi_{xr} \tag{96}$$

In a similar manner, one finds

$$\psi_{rr} = \frac{1}{\lambda}\left[\left(\frac{d\psi_r}{dx}\right)_{char} - \psi_{xr}\right] \tag{97}$$

If one substitutes Eqns 96 and 97 into Eqn 90 and performs some algebraic manipulations, the following relations can be derived:

$$\text{on } \frac{dr}{dx} = \lambda_1; \quad \frac{d\psi_x}{dx} + \lambda_2 \frac{d\psi_r}{dx} - \frac{D}{A} = 0 \tag{98}$$

$$\text{on } \frac{dr}{dx} = \lambda_2; \quad \frac{d\psi_x}{dx} + \lambda_1 \frac{d\psi_r}{dx} - \frac{D}{A} = 0 \tag{99}$$

Using Eqn 75 one can write

$$\psi_r = r(2h_o - V^2)^{\frac{1}{\gamma-1}} V\cos\theta \tag{100}$$

Differentiation yields

$$\frac{d\psi_r}{dx} = [2h_o - V^2]^{\frac{1}{\gamma-1}} \left\{ -rV\sin\theta \frac{d\theta}{dx} + r\cos\theta \frac{dV}{dx} + \right.$$

$$\left. + \frac{r}{\gamma-1} \frac{V\cos\theta}{2h_o - V^2} \frac{d}{dx}(2h_o - V^2) + \lambda V\cos\theta \right\} \tag{101}$$

Similarly one obtains

$$\frac{d\psi_x}{dx} = (2h_o - V^2)^{\frac{1}{\gamma-1}} \left\{ -rV\cos\theta \frac{d\theta}{dx} - r\sin\theta \frac{dV}{dx} - \right.$$

$$\left. - \frac{r}{\gamma-1} \frac{V\sin\theta}{2h_o - V^2} \frac{d}{dx}(2h_o - V^2) - \lambda V\sin\theta \right\} \tag{102}$$

If one substitutes Eqns 101 and 102 into Eqns 98 and 99, it can be shown, after a considerable amount of algebra, that the equations along the characteristics can be expressed as

$$\text{on } \frac{dr}{dx} = \tan(\theta \pm \mu) \tag{103}$$

$$\frac{1}{V}\frac{dV}{dx} \mp \tan\mu \frac{d\theta}{dx} - \frac{\tan(\theta \pm \mu)\tan^2\mu}{r} - \frac{\tan^2\mu}{a^2}\frac{dh_o}{dx} - \frac{(2h_o - V^2)^{-\frac{1}{\gamma-1}}\tan^2\mu}{rV\cos\theta[\tan\theta - \tan(\theta \pm \mu)A}\frac{D}{A} = 0 \tag{104}$$

Introducing D and A from Eqn 89 (by comparison with Eqn 90), one can obtain the final characteristic equations.

$$\text{on} \quad \frac{dr}{dx} = \tan(\theta \pm \mu) \tag{105}$$

$$\frac{1}{V}\frac{dV}{dx} \mp \tan\mu\frac{d\theta}{dx} - \frac{\sin\mu\sin\theta\tan\mu}{r\cos(\theta \pm \mu)} + \frac{\sin^3\mu}{\gamma\cos(\theta \pm \mu)}\frac{d}{dn}\left(\frac{S}{R}\right) - \frac{\sin^3\mu}{a^2\cos(\theta \pm \mu)}\frac{dh_o}{dn} = 0 \tag{106}$$

The upper sign in Eqns 105 and 106 refer to the so-called left-running characteristic while the lower sign refers to the right-running characteristic.

If one multiplies Eqn 106 by dx and notes that

$$\frac{dx}{dn} = \frac{\cos(\theta \pm \mu)}{\sin \mu} \tag{107}$$

Equation 106 becomes:

$$\frac{dV}{V} \mp \tan\mu \, d\theta - \frac{\sin\mu \sin\theta \tan\mu}{\sin(\theta \pm \mu)} \frac{dr}{r} +$$

$$+ \frac{\sin^2\mu}{\gamma} d\left(\frac{S}{R}\right) - \frac{1}{V^2} dh_o = 0 \tag{108}$$

If Eqn 108 is integrated along a characteristic from Point 1 to Point 2, and if the average value of the coefficients for each term are used, Eqn 108 becomes (noting $h_o = c_p T_o$)

$$\ln \frac{V_2}{V_1} \mp \tan\bar{\mu}_{12}(\theta_2 - \theta_1) - \frac{\sin\bar{\mu}_{12} \sin\bar{\theta}_{12} \tan\bar{\mu}_{12}}{\sin(\overline{\theta \pm \mu})_{12}} \ln \frac{r_2}{r_1} +$$

$$+ \frac{\sin^2\bar{\mu}_{12}}{\gamma} \left[\left(\frac{S}{R}\right)_2 - \left(\frac{S}{R}\right)_1\right] - \frac{c_p(T_{o2} - T_{o1})}{\bar{V}_{12}^2} = 0 \tag{109}$$

All quantities with a "bar" over them and subscript 12 represent average values between Points 1 and 2 on a characteristic curve. Once again it should be remembered that the upper signs are used for the left running characteristics while the lower signs are for the right-running characteristics.

2. Computational Procedure

A detailed discussion of the computation in the shock layer flow field, such as the location of shock points,

net points, body points, and the properties along an initial right-running characteristic is presented in Vol II of this report. A brief description of the flow field computation has been included in this section to provide a better understanding of the characteristic and compatability equations. As described earlier, the non-uniform supersonic wake flow field, which is known either from an analytical approach (Section II) or from experiments, provides effective upstream boundary conditions; the Rankine-Hugonoit relations, when applied locally across the shock, determine the flow properties immediately behind the shock. With an attached curved shock at the apex of the secondary body, the shock layer, the region between the shock and body surface, will have rotational, non-homoenergic characteristics. The analysis using the method of characteristics is valid in the shock layer provided the flow field is completely supersonic.

In order to proceed with the computation of the flow field by the method of characteristics, it is necessary to know the flow properties along an initial right running characteristic. In the case of an attached shock, it is usually assumed that a small conical flow region exists at the apex of the body. The shock angle, related to the semi-apex angle of the body and the centerline upstream Mach number, and the flow properties in the conical flow region are determined from Taylor-Maccoll conical flow relationships. Since the local characteristic direction is inclined at the local Mach angle from the local flow direction, the initial right running characteristic can be constructed from the knowledge of the local Mach number and local flow direction in the conical flow region. The computation along any right running characteristic is carried out from a shock point to a body point. Knowing the location and flow properties at a shock point, net points, and a body point on one right running characteristic, the location and flow properties at field points on the next right running characteristics are determined using shock jump conditions, characteristic compatability conditions, and body boundary conditions.

A new shock point is fixed by using the shock point and the net point on the previous right running characteristic and Rankine-Hugonoit shock jump conditions. An iteration procedure has to be adapted to fix the new shock point.

A new net point is located using the previously located shock point and net point, two net points, or net point and body point, depending on the region of desired new net point. In addition, the streamline passing through the net point in search must be located on the previous right running characteristic to determine the total temperature and entropy at the new net point. The velocity and flow

direction at the new net point are determined from two characteristic compatability relations (Eqn 109).

Since the body surface is a streamline, the total temperature and entropy remain constant along the body surface. From body boundary conditions the flow direction at any point on the body surface is along the tangent direction to the surface at that point. The new body point is located using the previously determined body point and net point. The compatability relation along the right running characteristic provides the magnitude of the surface velocity. The temperature and static pressure are determined from the isentropic relations

$$T = T_o - \frac{V^2}{2 C_p} \tag{110}$$

$$\frac{p}{p_\infty} = \frac{\left(\frac{T}{T_\infty}\right)^{\gamma/\gamma-1}}{Exp\left[\left(\frac{S}{R}\right) - \left(\frac{S}{R}\right)_\infty\right]} \tag{111}$$

Then the local velocity, flow direction, total temperature and entropy are sufficient to determine all other flow properties at any point.

C. Limits of and Assumptions in the Secondary Body Analysis

1. Limits of the Secondary Body Analysis

The primary and obvious limitation is that, since a characteristic method is used, it is limited to supersonic velocities. The most important implications of this fact are that the secondary body must have an attached bow shock and the analysis will only extend along the body to the sonic line. Although this limitation is, in a certain sense, severe, there is yet a large number of bodies to which the method will apply.

A second limitation of the method is that the wake of the secondary body is not analyzed. The result of this is that base pressures must be obtained from another source to obtain a complete pressure distribution for a drag coefficient calculation.

2. Assumptions in the Method

Two main assumptions are made in using the method: first, it is assumed that a boundary layer analysis is not needed to obtain the desired results, and second, that a reasonably sized decelerator tow line will not invalidate the calculation with an attached shock.

The omission of a boundary layer analysis should not lead to any significant error in the results obtained. For bodies and regimes to which the method applies, boundary layer thicknesses are quite small compared to body dimensions, and the friction drag is a small percentage of pressure drag. The primary need for a boundary layer analysis would be for wake calculations.

At the very early stages of this investigation wind tunnel studies were conducted to examine the effects of simulated axial tow lines on the secondary body bow shock shape and pressure distribution. Figure 14 compares the shapes of bow shock waves on a 4-in diameter 30° half-angle cone in the wake of the 2-in diameter cone-cylinder forebody with and without two different simulated tow lines. As shown in Fig 14 the bow shocks with the simulated tow lines are obviously not attached, but the region of difference is very small, and the shock rapidly approaches that of the no-tow-line configuration. Pressure distribution studies were also conducted for this same cone with and without a tow line, and the results are shown in Fig 15. It can be seen that the simulated tow lines have nearly no effect on the pressure distribution.

It should be noted that one effect of the simulated tow line was not directly investigated. This effect is that, for a thickness equal to that of the tow line, there exists a wake velocity boundary condition of $V = 0$. This was not considered in either the wake analysis or the secondary body analysis. This condition will exist in any towed decelerator application, but the effects of neglecting it cannot be isolated in the results of this study.

D. Experimental Comparisons

In order to check the results of a sample calculation using the analysis, experiments were conducted to measure secondary body bow shock shape and surface pressure distribution. These tests were conducted at the University of Minnesota's Rosemount Aeronautical Laboratories in a 12 in x 12 in blow-down wind tunnel at $M_\infty = 3.0$. Figure 16 is a schematic of the installation and Fig 17 shows the 30° half-angle cone used as the secondary body. The primary body had the same

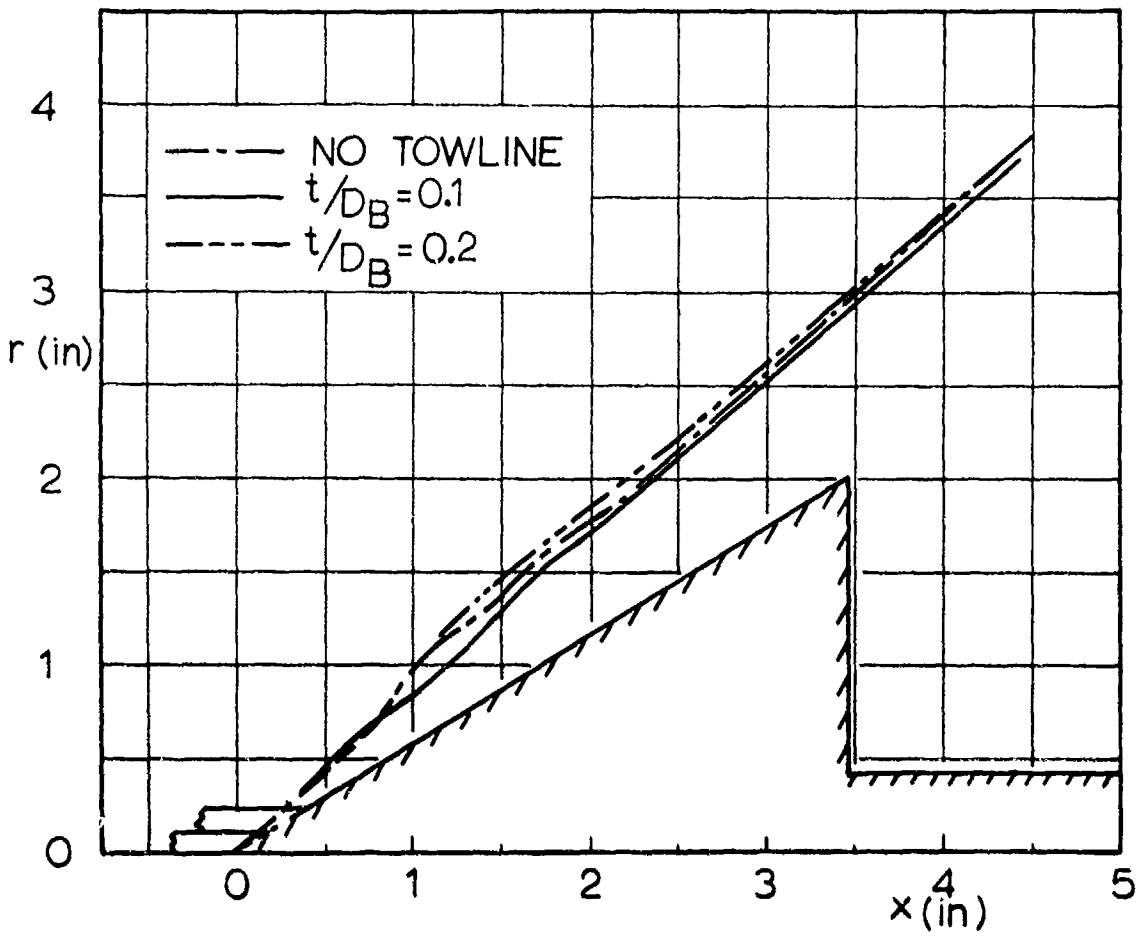

Fig 14 Comparison of Bow Shock Wave Shapes with and without two Simulated Towline Diameters at $\ell / D_B = 5$, $M_\infty = 2.98$

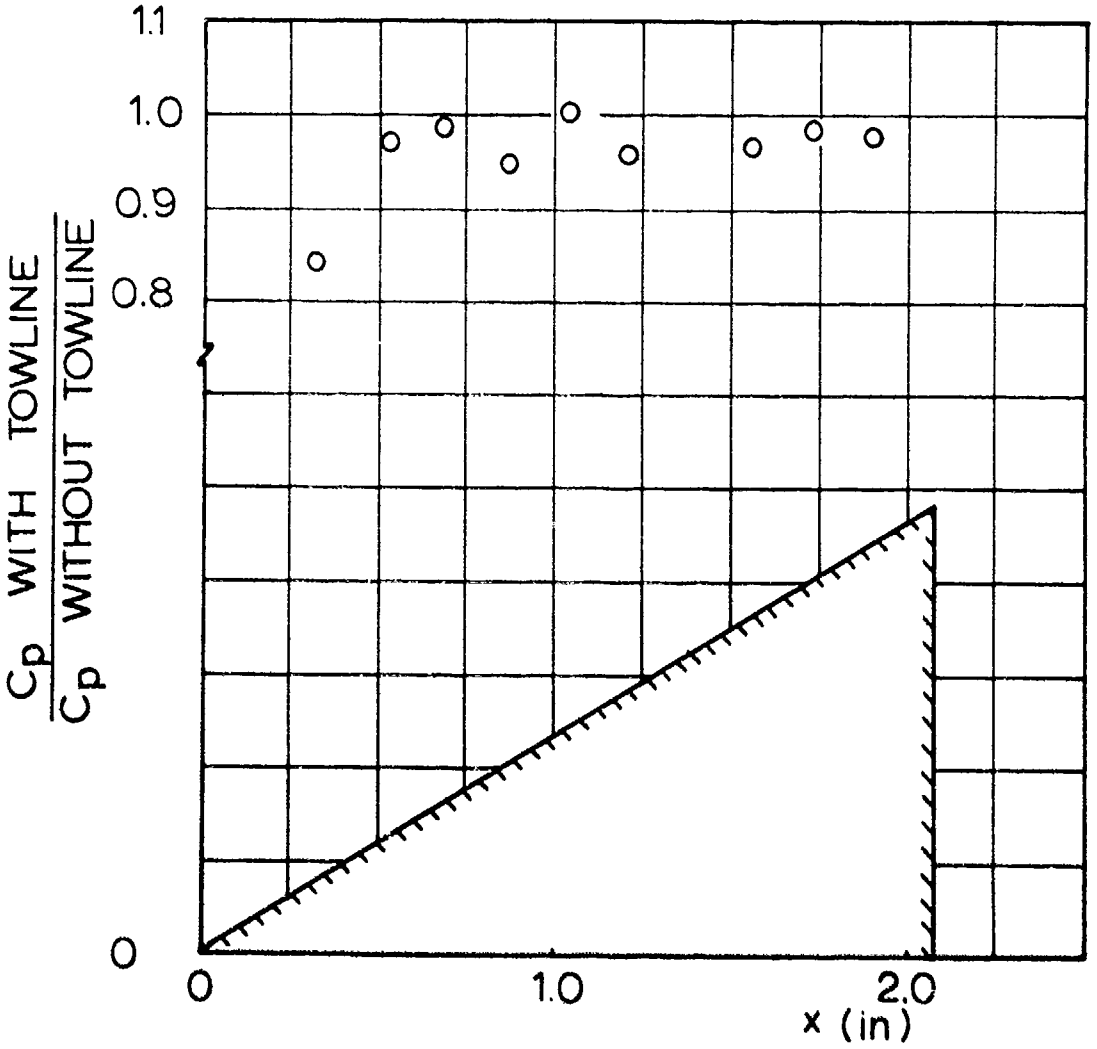

Fig 15 Pressure Distribution on a 30° Half-Angle Cone $\ell/D_B=5$, $M_\infty=2.98$

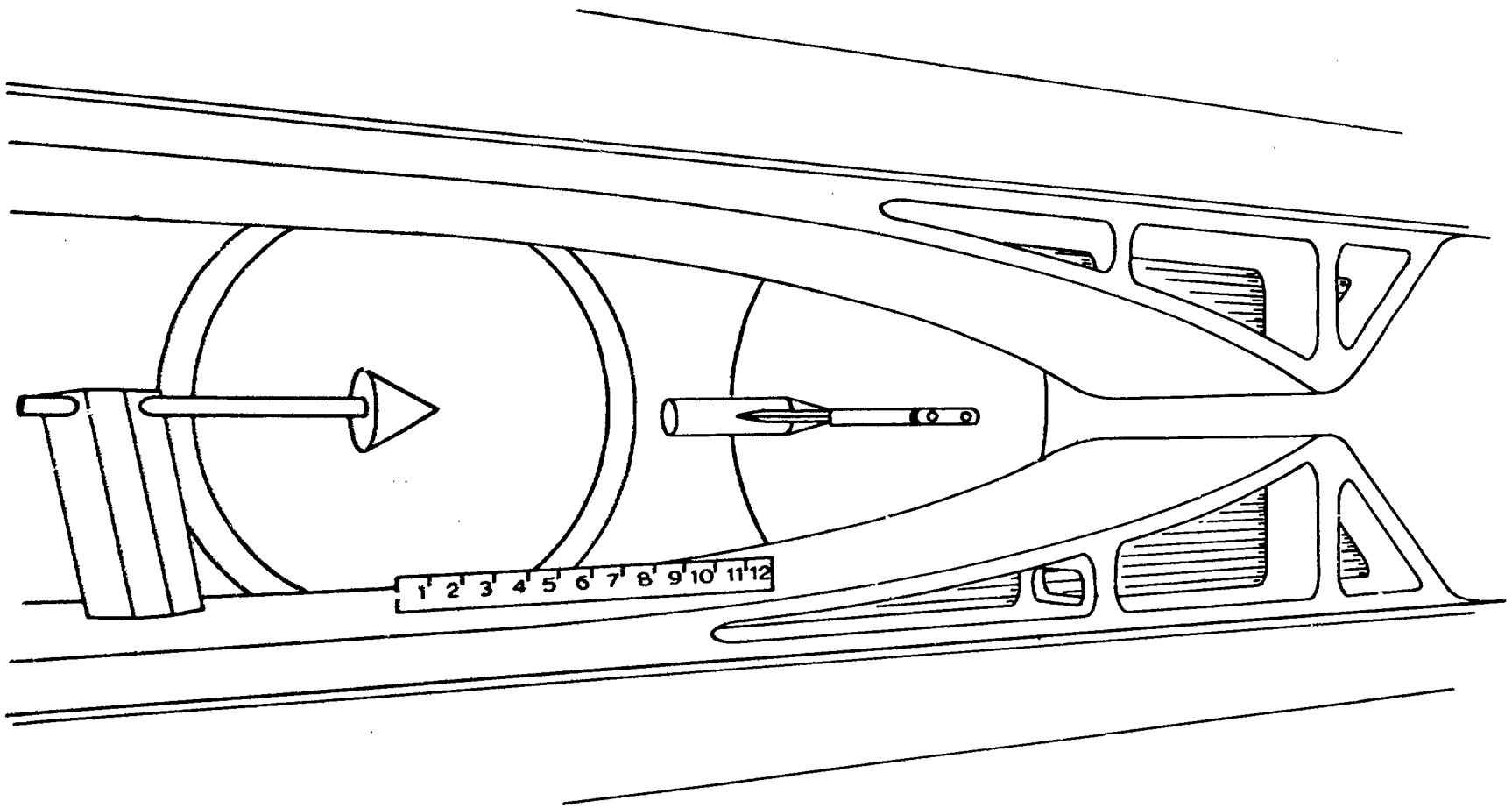

Fig 16 Secondary Body Installed in Wake of Forebody at U of M Wind Tunnel

ALL DIMENSIONS IN INCHES

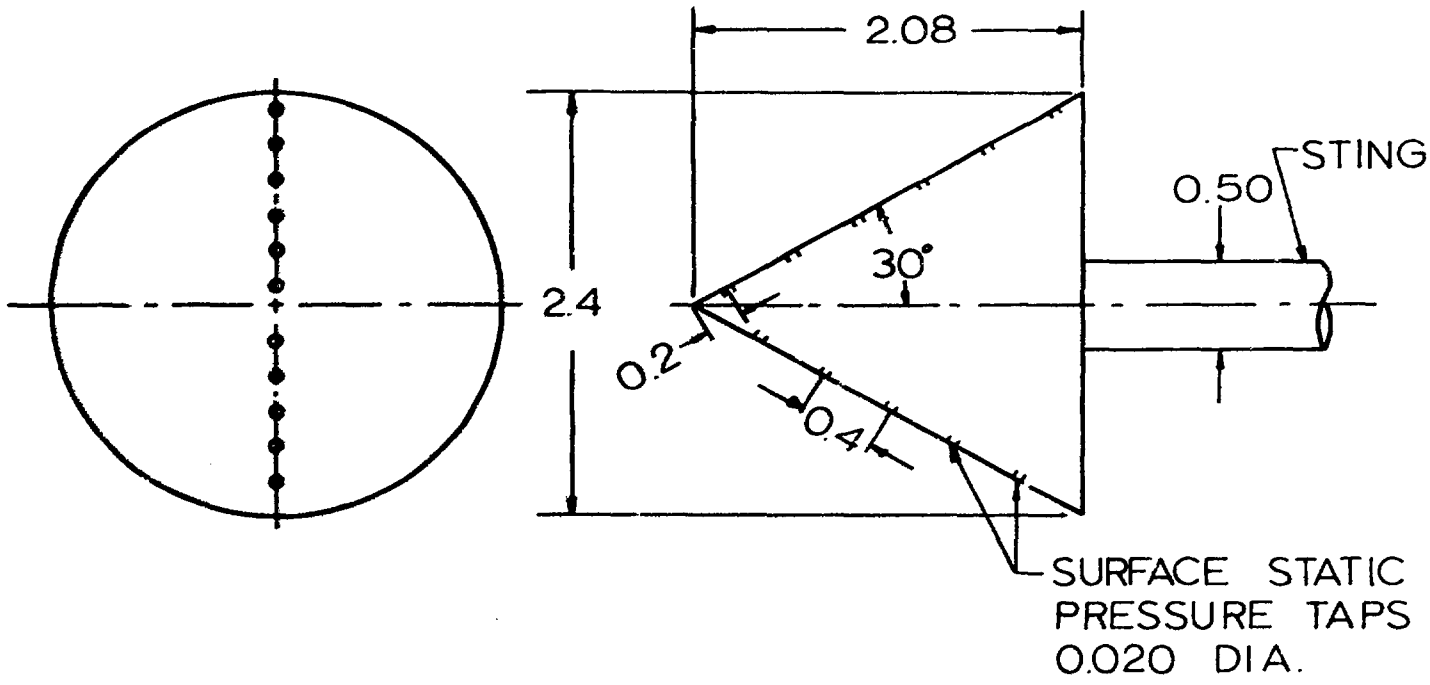

Fig 17 30° Half-Angle Cone Pressure Model of Secondary Body

geometry as the 1.2-in diameter cone-cylinder body examined in Section II, and the tests were conducted at the same conditions. Measured shock shapes and surface pressure distributions were non-dimensionalized with the 2.4-in diameter cone and converted to shapes and distributions for the 4.0-in diameter cone. This was done to allow direct comparison with the theoretical results for the 4-in diameter cone and 2-in base diameter cone-cylinder forebody.

Generally, in the comparisons that follow, two different calculations of the various parameters were made. The first calculation was made using wake data obtained from measurements (Ref 8), and the second, used wake data resulting from the forebody wake analysis. This was done in order to provide a check of the secondary body analysis in which all the inputs to the analysis are as accurate as possible. It is shown in the following sections that better agreement is obtained using measured rather than calculated wake data.

1. Secondary Body Bow Shock Shape

Shock shape measurements were made at ℓ/D_B's of 5, 7, and 9 (Figs 18, 19, 20). At an ℓ/D_B of 5 experimental data was not available, so the comparison only compares measured and calculated points using the primary body analysis. The agreement at ℓ/D_B's of 7 and 9 between measured values and values using measured wake data is excellent, very nearly exact. The agreement with the purely calculated shock shape is not as close, but must be called good.

2. Surface Pressure Distribution

Pressure distributions were also measured at ℓ/D_B's of 5, 7, and 9, as shown in Figs 21, 22, and 23. Again the agreement is best with the calculations using the experimental wake data, being within 10% or better. The effects of the calculated wake being too narrow are seen in the C_p results based on this, in that the C_p's rise too rapidly from the lower values in the front of the cone. It appears that, if the width of the predicted wake was adjusted, the agreement could be brought into the 10% region.

3. Pressure Drag Coefficients

Calculated and measured drag coefficients are shown in Fig 24. In general the calculated drag coefficients are 11% higher than measured, and the difference between values using measured or calculated wake conditions is quite small.

A measured base pressure coefficient of $C_p = -0.074$ was used to obtain the pressure drag coefficients.

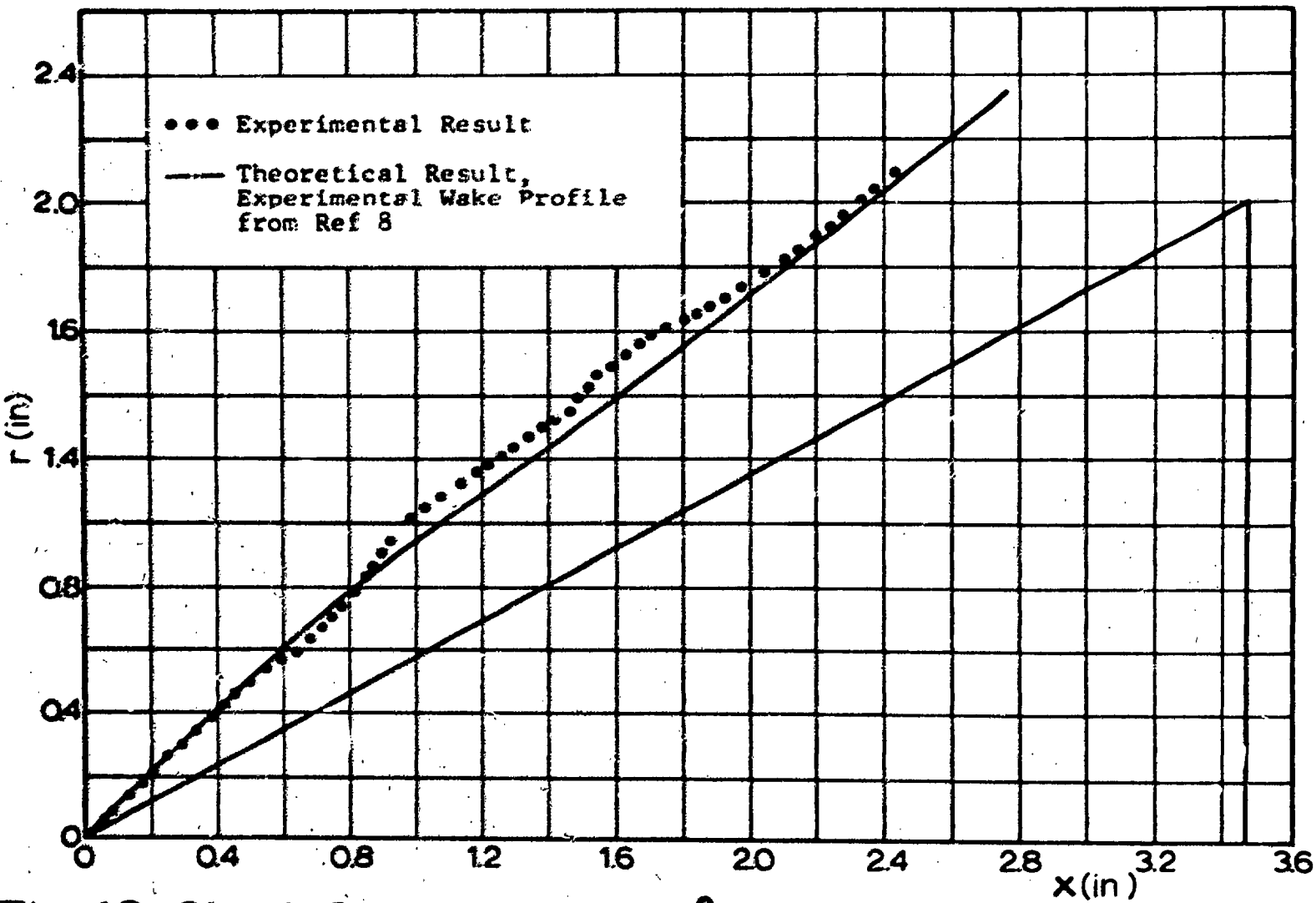

Fig 18 Shock Shapes for a 30° Half-Angle Cone in the Wake of the Forebody at $\ell/D_B = 5.0$, $M_\infty = 2.98$

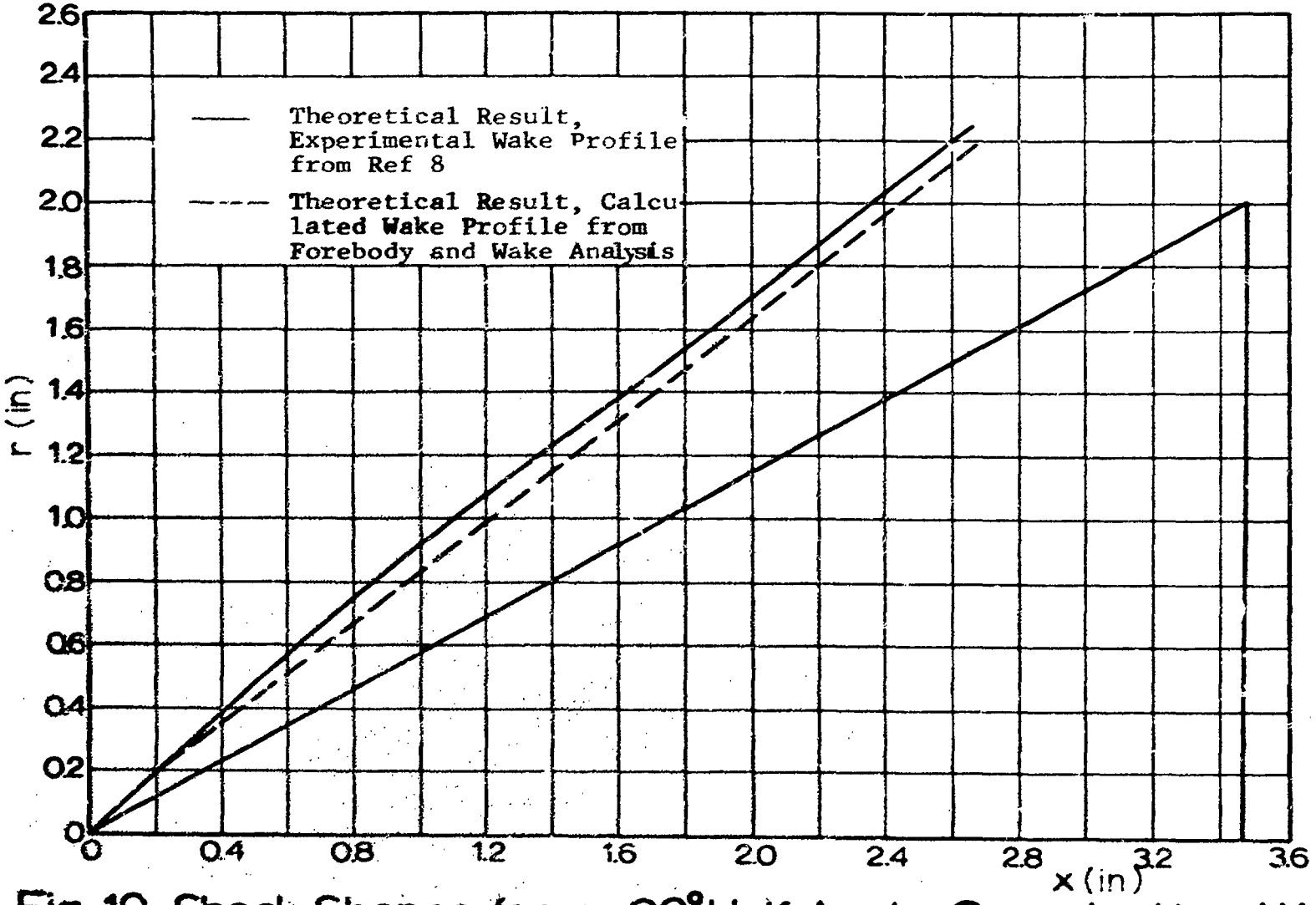

Fig 19 Shock Shapes for a 30° Half-Angle Cone in the Wake of the Forebody at $\ell/D_B = 7.0$, $M_\infty = 2.98$

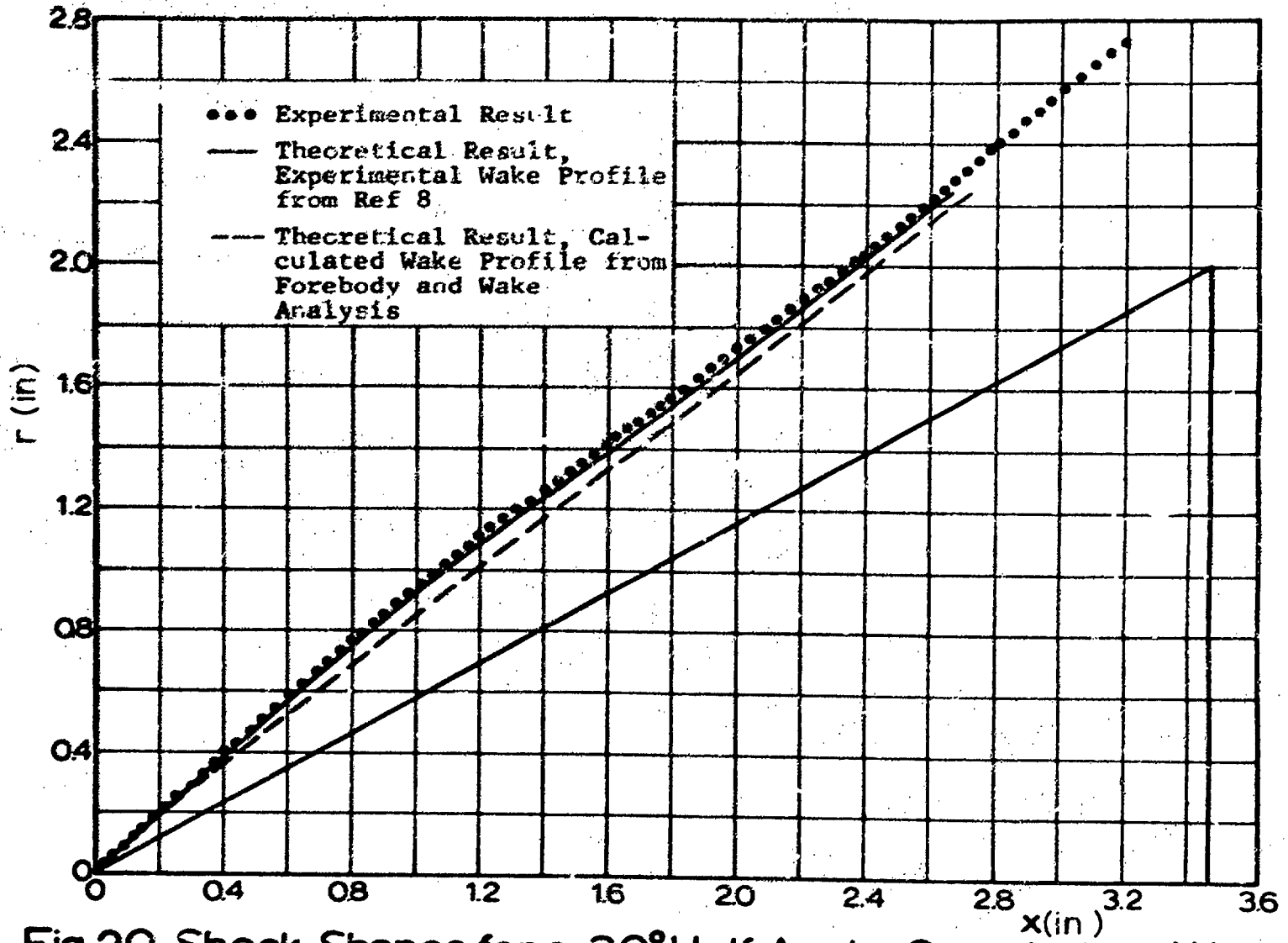

Fig 20 Shock Shapes for a 30° Half-Angle Cone in the Wake of the Forebody at ℓ/D_B =9.0, M_∞ = 2.98

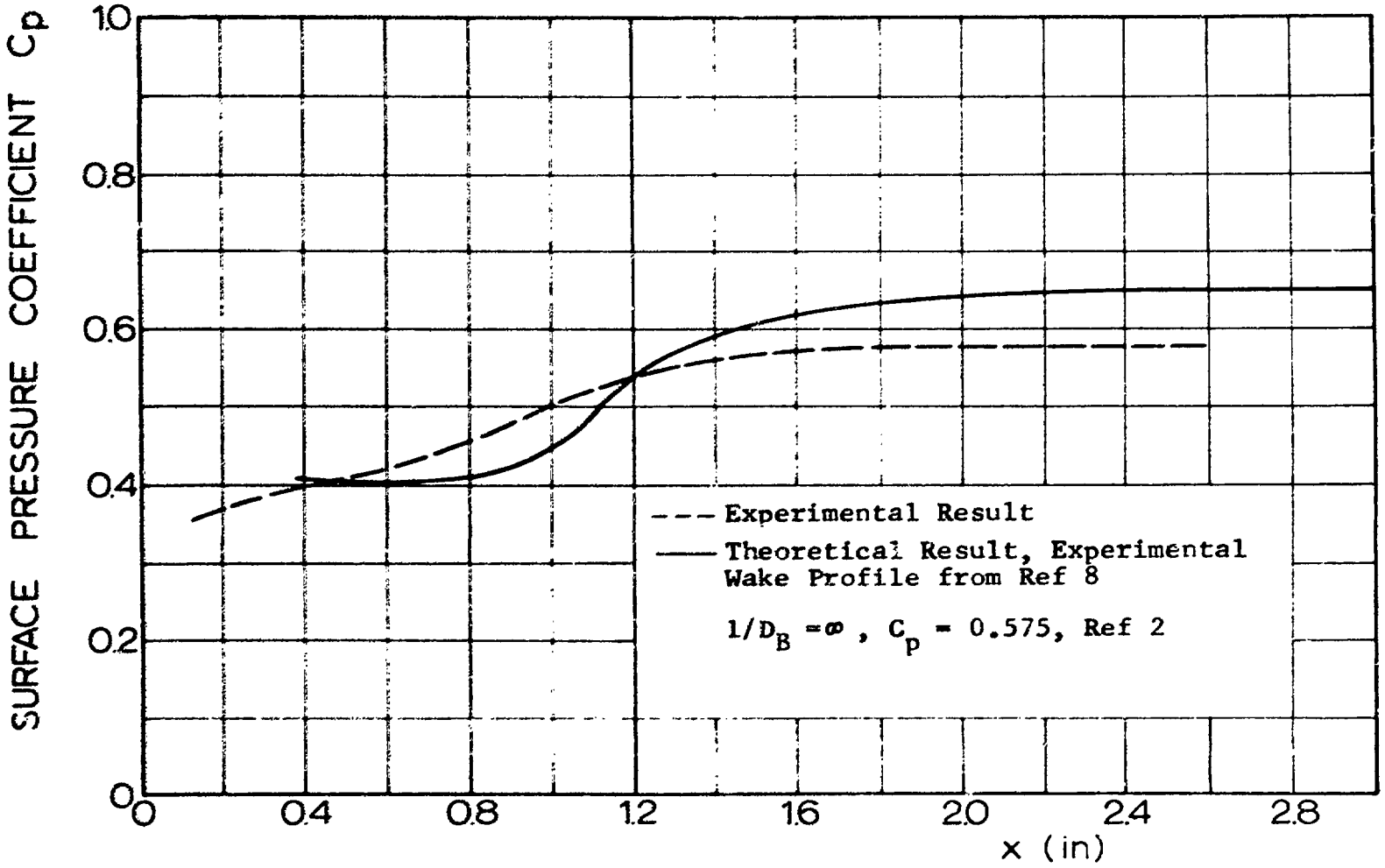

Fig 21 Surface Pressure Coefficient vs Axial Distance for a 30° Half-Angle Cone Behind a 26° Cone-Cylinder, $\ell / D_B = 5.0$, $M_\infty = 2.98$

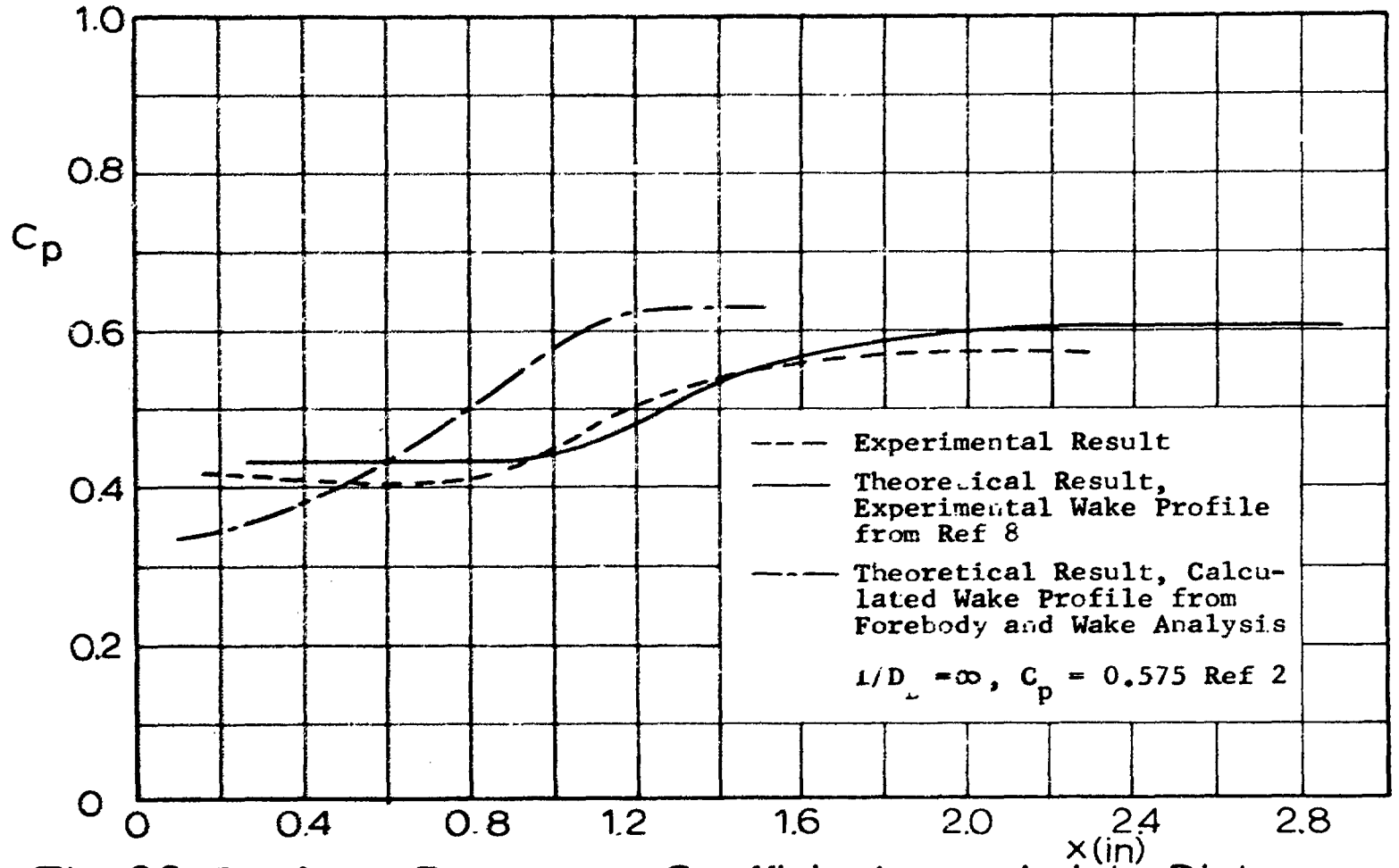

Fig 22 Surface Pressure Coefficient vs Axial Distance for a 30° Half-Angle Cone Behind a 26° Cone-Cylinder $\ell / D_B = 7.0$, $M_\infty = 2.98$

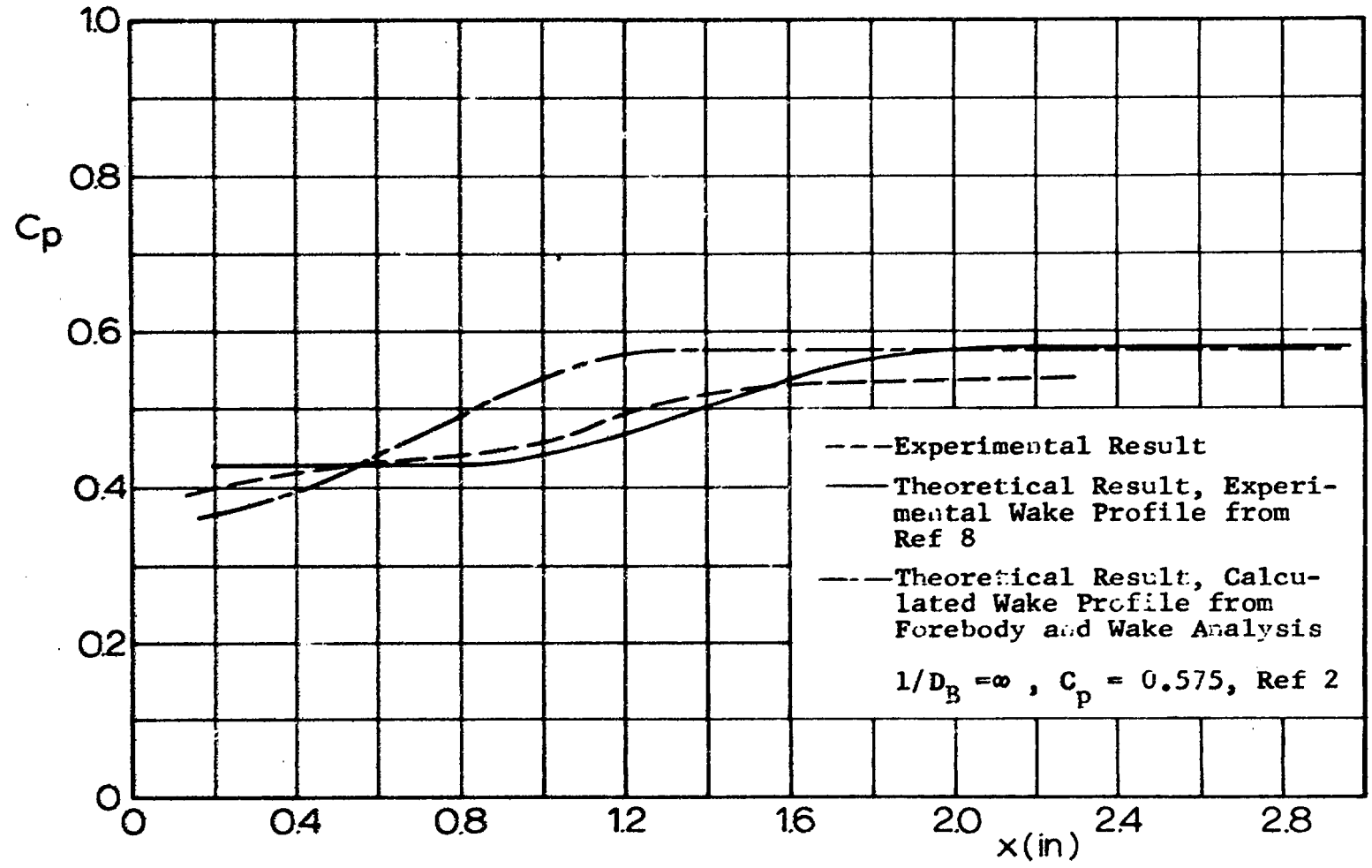

Fig 23 Surface Pressure Coefficient vs Axial Distance for a 30° Half-Angle Cone Behind a 26° Cone-Cylinder $\ell / D_B = 9.0$, $M_\infty = 2.98$

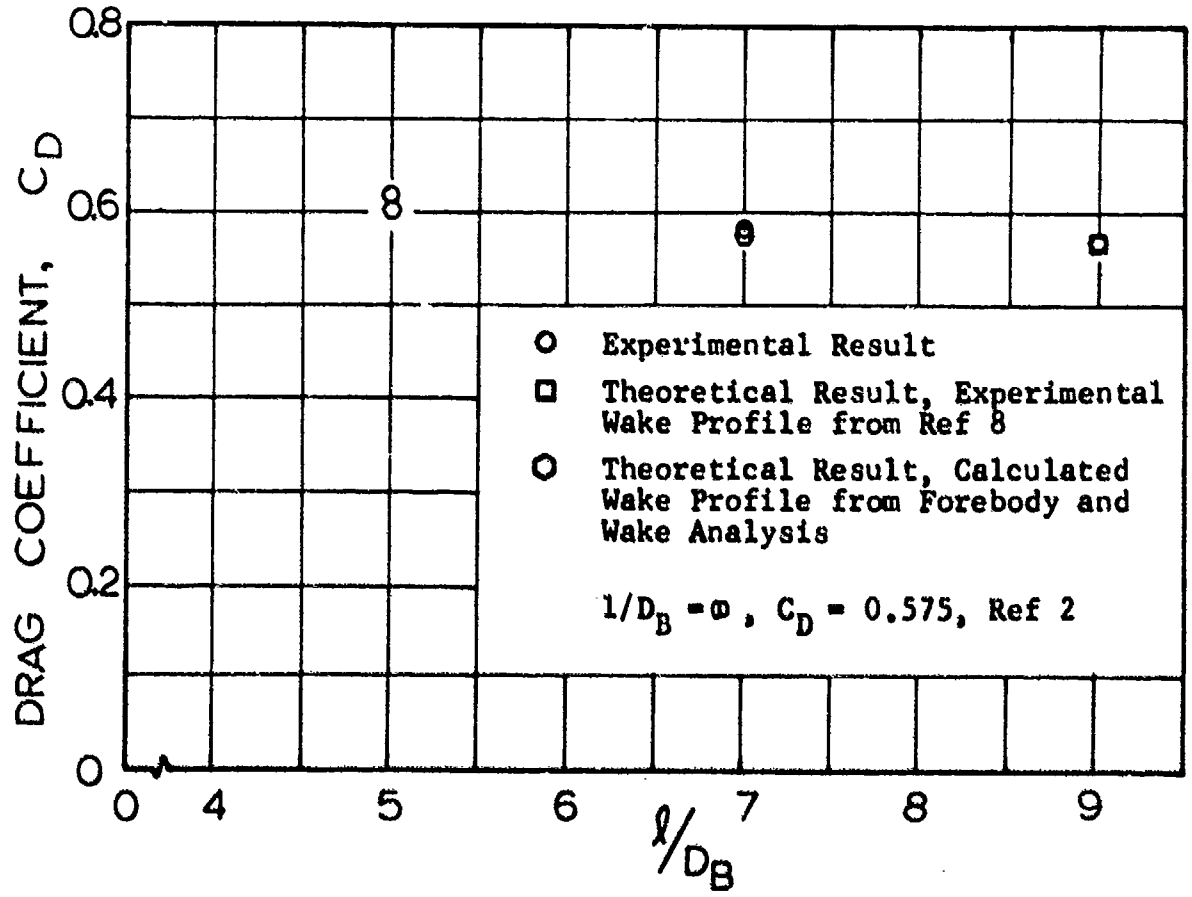

Fig 24 Pressure Drag Coefficient vs l/D_B for 30° Half-Angle Cone Behind a 26° Cone-Cylinder, $M_\infty = 2.98$

IV. SUMMARY

Methods of analysis have been developed for calculating flow field properties of certain classes of two-body decelerator systems in supersonic flow. In this volume the analytical techniques used for the forebody and secondary bodies have been explained, and the results of a sample calculation compared with experimental measurements. In general, the comparison was quite good; differences between calculated and measured values were on the order of 10%.

Thus methods and procedures exist for calculating the significant flow field properties of the two body system with reasonable engineering accuracy. In achieving this the information about the flow field required for the calculations has been kept to the smallest amount possible at this time. However, two things are needed in order to calculate, namely, the forebody bow shock shape and the secondary body base pressure. These two items can easily be determined experimentally, or can be approximated quite well for initial calculations.

In conclusion, a large step has been made in enabling calculation of the performance of certain supersonic decelerators. Certain improvements and refinements can and should be made, but the broad framework and basic calculations have been established making modifications possible.

REFERENCES

1. Henke, D. W.: "Establishment of an Unsymmetrical Wake Test Capability for Aerodynamic Decelerators," AFFDL-TR-67-192, Vol. II, August, 1968.

2. Ames Research Staff: "Equations, Tables, and Charts for Compressible Flow," NACA Report 1135, 1953.

3. Reshotko, E., and Tucker, M.: "Approximate Calculation of the Compressible Turbulent Boundary Layer with Heat Transfer and Arbitrary Pressure Gradient," NACA Report TN 4154, December 1957.

4. Zakky, V., and Fox, H.: "An Experimental and Theoretical Investigation of the Turbulent Far Wake," AIAA Journal Vol 5, No. 3, March 1967, pp. 568-574.

5. Pallone, A., Erdos, J., and Eckermann, J.: "Hypersonic Laminar Wakes and Transition Studies," AIAA Journal, Vol. 2, No. 5, May 1964, pp. 855-863.

6. Shapiro, A. H.: The Dynamics and Thermodynamics of Compressible Fluid Flow, Ronald Press Co., New York, 1954, Vols. 1 and 2.

7. Henke, D. W.: "Establishment of an Unsymmetrical Wake Test Capability for Aerodynamic Decelerators," AFFDL-TR-67-192, Vol. I, August, 1968.

8. Arnold Engineering Development Center, Von Karman Gas Dynamics Facility, Unpublished wake survey data behind the 2-in diameter cone cylinder forebody, using the test facility, test hardware, forebody supports, and wake survey probes (WT-IIA) described in Appendix V of Reference 1 above.

Unclassified

Security Classification

DOCUMENT CONTROL DATA - R & D

(Security classification of title, body of abstract and indexing annotation must be entered when the overall report is classified)

1. ORIGINATING ACTIVITY *(Corporate author)*

University of Minnesota
Minneapolis, Minn. 55455

2a. REPORT SECURITY CLASSIFICATION

Unclassified

2b. GROUP

3. REPORT TITLE

Analysis of the Supersonic Flow Field About a Forebody-Decelerator Combination, Vol. I, Theoretical Methods and Result Comparisons

4. DESCRIPTIVE NOTES *(Type of report and inclusive dates)*

Final Report - December 1967 - October 1969

5. AUTHOR(S) *(First name, middle initial, last name)*

R. A. Noreen
L. W. Rust, Jr.
P. P. Rao

6. REPORT DATE	7a. TOTAL NO. OF PAGES	7b. NO. OF REFS
March 1972	63	8

8a. CONTRACT OR GRANT NO.

F33615-68-C-1227

b. PROJECT NO. 6065

c. Task No. 606503

d.

9a. ORIGINATOR'S REPORT NUMBER(S)

9b. OTHER REPORT NO(S) *(Any other numbers that may be assigned this report)*

AFFDL-TR-71-35, Vol. I

10. DISTRIBUTION STATEMENT

Distribution limited to U.S. Gov't Agencies only; Test and Evaluation; 10 September 1971. Other requests for this document must be referred to AFFDL/FER, WPAFB, Ohio 45433

11. SUPPLEMENTARY NOTES

12. SPONSORING MILITARY ACTIVITY

AFFDL/FER
WPAFB, Ohio 45433

13. ABSTRACT

The supersonic flow field about a forebody-decelerator combination is analyzed. Tangent-cone and Newtonian methods are used to predict forebody surface pressures. Empirical correlations based on local similarity solutions predict the boundary layer characteristics, and boundary layer similarity techniques are used to predict the forebody wake parameters. The flow about a conical secondary body in the forebody wake is calculated using the method of characteristics. In Volume I the methods are presented and explained, and the results of the calculations are compared with experimental measurements; in Volume II the details of the calculation procedure and computer program are presented.

DD FORM 1 NOV 1473

Unclassified

Security Classification

Unclassified
Security Classification

14. KEY WORDS	LINK A		LINK B		LINK C	
	ROLE	WT	ROLE	WT	ROLE	WT
Wake Supersonic Flow Field Decelerator Boundary Layer Pressure Distribution						

*U S Government Printing Office: 1972 — 759-083/400

Security Classification